PHYSICAL REVIEW D **75,** 035002 (2007)

Mass spectrum in R-parity violating minimal supergravity and benchmark points

B. C. Allanach*
DAMTP, University of Cambridge, Cambridge, UK

M. A. Bernhardt† and H. K. Dreiner‡
Physics Institute, University of Bonn, Bonn, Germany

C. H. Kom§
DAMTP, University of Cambridge, Cambridge, UK

P. Richardson‖
IPPP, University of Durham, Durham, UK
(Received 3 October 2006; published 5 February 2007)

We investigate in detail the low-energy spectrum of the R-parity violating minimal supergravity model using the computer program SOFTSUSY. We impose the experimental constraints from the measurement of the anomalous magnetic moment of the muon, $(g-2)_\mu$, the decay $b \to s\gamma$ as well as the mass bounds from direct searches at colliders, in particular on the Higgs boson and the lightest chargino. We also include a new calculation for the R-parity violating contribution to $\mathrm{Br}(B_s \to \mu^+\mu^-)$. We then focus on cases where the lightest neutralino is *not* the lightest supersymmetric particle (LSP). In this region of parameter space either the lightest scalar tau (stau) or the scalar tau neutrino (tau sneutrino) is the LSP. We suggest four benchmark points with typical spectra and novel collider signatures for detailed phenomenological analysis and simulation by the LHC collaborations.

DOI: 10.1103/PhysRevD.75.035002 PACS numbers: 12.60.Jv, 04.65.+e, 14.80.Ly

I. INTRODUCTION

The most widely discussed solution to the gauge hierarchy problem [1] of the standard model of particle physics (SM) [2] is the supersymmetric extension of the SM (SSM) [3]. However, no supersymmetric particle has been observed to-date. Thus if it exists supersymmetry (SUSY) must be broken and the mass scale should be of order the TeV energy scale, in order to maintain the solution to the hierarchy problem [4]. The TeV energy realm will be probed at the LHC starting in 2007 with the search for SUSY of paramount interest [5].

The general SSM renormalizable superpotential with minimal particle content is given by [6]

$$W_{\mathrm{SSM}} = W_{\mathrm{P}_6} + W_{\not{\mathrm{P}}_6}, \tag{1}$$

$$W_{\mathrm{P}_6} = \epsilon_{ab}[(\mathbf{Y_E})_{ij} L_i^a H_1^b \bar{E}_j + (\mathbf{Y_D})_{ij} Q_i^{ax} H_1^b \bar{D}_{jx} + (\mathbf{Y_U})_{ij} Q_i^{ax} H_2^b \bar{U}_{jx} + \mu H_1^a H_2^b], \tag{2}$$

$$W_{\not{\mathrm{P}}_6} = \epsilon_{ab}[\tfrac{1}{2}\lambda_{ijk} L_i^a L_j^b \bar{E}_k + \lambda'_{ijk} L_i^a Q_j^{bx} \bar{D}_{kx}] + \epsilon_{ab}\kappa^i L_i^a H_2^b + \tfrac{1}{2}\epsilon_{xyz}\lambda''_{ijk}\bar{U}_i^x \bar{D}_j^y \bar{D}_k^z. \tag{3}$$

Here we have employed the notation of Ref. [7]. We have split the superpotential into two sets of interactions, for reasons which we shall explain shortly.

If simultaneously present, the baryon and lepton number violating interactions in Eq. (3) lead to rapid proton decay [8]. Therefore the SSM must be augmented by a symmetry. The most widely studied scenario is R-parity [9], for which $W_{\not{\mathrm{P}}_6} = 0$. However, it suffers from dangerous dimension-five proton-decay operators [6]. This is solved by proton hexality, P_6, an anomaly-free $\mathbf{Z}_6$ discrete gauge symmetry [10]. The renormalizable superpotential terms are equivalent to conserved R-parity, namely W_{P_6}, but the dimension-five proton-decay operators are forbidden. So we consider this the more appropriate choice and have correspondingly labeled the superpotential in Eqs. (1) and (2). The P_6-SSM is conventionally denoted the minimal supersymmetric standard model (MSSM).

Baryon triality, B_3 is an anomaly-free $\mathbf{Z}_3$ discrete gauge symmetry [11], which prohibits the $\overline{U}\,\overline{D}\,\overline{D}$ interactions, thereby stabilising the proton. It is thus theoretically equally well motivated to P_6. A third possibility to stabilize the proton is lepton parity [11], which prohibits the lepton-number violating interactions in Eq. (3). However, lepton parity is anomalous [11]. As the alternative to the P_6-MSSM we shall focus on the phenomenological analysis of baryon triality at colliders. However, we shall also consider some implications of lepton parity.

The P_6-MSSM mass spectrum and couplings have been studied in great detail [12–14]. However, there are two

*Email: allanach@cern.ch
†Email: markus@th.physik.uni-bonn.de
‡Email: dreiner@th.physik.uni-bonn.de
§Email: c.kom@damtp.cam.ac.uk
‖Email: Peter.Richardson@durham.ac.uk

reasons why it is highly desirable to perform analyses of the *general* SSM at colliders. First, to make sure that no possibility to discover SUSY is left untried. If we focus our endeavours on one specific form of SUSY, due to theoretical prejudice, for example, then we might initially entirely miss the discovery. Second, SUSY is not a simple extension of the SM, like for example right-handed neutrinos, which does not affect most parts of the model. In the SSM, the particle spectrum is more than doubled. If the SSM is to provide a solution to the technical hierarchy problem, we expect all of the new particles to have masses $\lesssim \mathcal{O}(2\ \mathrm{TeV})$. Thus if low-energy SUSY exists we should expect many new processes to be kinematically accessible at the LHC. When considering a specific SUSY process as a signature, many other SUSY processes will act as background and must be taken into account [15].

Thus in order to perform simulations of signatures involving the complete supersymmetric spectrum in preparation for the LHC, we restrict ourselves to specific points of the P_6 minimal supergravity (P_6-mSUGRA) parameter space. Over the years several such example points have been proposed [15–17]. Some of these "benchmark points" have been excluded by searches at LEP, for example, the points 3 and 5 in Ref. [15]. Some points are strongly motivated by the resulting cosmological relic density [18]. A set of benchmark points and parameter lines in the mSUGRA parameter space have been agreed upon, the Snowmass points and slopes (SPS) [17]. The resulting spectra have been compared for various numerical RGE integration codes [19,20] and have been investigated both in the context of the LHC and the ILC. It is our purpose to facilitate the extension of this work to the $\not{P}_6$-MSSM. As a first step, we shall investigate the mass spectrum and couplings in some detail. For further more detailed experimental studies we also propose a set of benchmark points.

In Sec. II we briefly review the most widely studied model, namely, the P_6-MSSM embedded in supergravity [21,22]. In order to throw a wider net in our search for SUSY, we extend this discussion to the $\not{P}_6$-MSSM in Sec. III, emphasizing the main differences to the P_6 conserving case and examining bounds on the $\not{P}_6$ couplings. In this first study we sometimes will focus on the simplest model of no-scale supergravity [23]. We examine constraints on $\not{P}_6$ mSUGRA parameter space arising from precision measurements in Sec. IV and the sparticle spectrum in Sec. V. We present the definition of the proposed mSUGRA benchmark points in Sec. VI, where we also detail the spectrum and sparticle decays. We summarize and conclude in section VII, following with expressions for the $\not{P}_6$ contribution to $\mathrm{Br}(B_{q_k} \to e_m^+ e_l^-)$ decays, a generalization of results in the literature in the appendix. In this paper we do not consider alternative mechanisms to communicate to the visible sector such as gauge or gaugino mediated SUSY breaking [24] or anomaly mediated SUSY breaking [25].

II. THE P_6-MSSM

The P_6-MSSM has 124 free parameters [26], and the $\not{P}_6$-MSSM more than 200. Such an extensive parameter space is intractable for a systematic phenomenological analysis at colliders. It is thus mandatory to consider simpler models, which represent the variety in the SSM. Hereby both observational hints [27] and theoretical considerations [28] have been employed as guiding tools.

Within the SSM, the unification of the three SM gauge couplings at a scale $M_X = \mathcal{O}(10^{16}\ \mathrm{GeV})$ [27] indicates the embedding in a unified model. The most widely studied and the simplest of these models is mSUGRA with conserved P_6 [28] and radiative electroweak symmetry breaking [29]. In this case, we are left with five free parameters

$$M_0, \qquad M_{1/2}, \qquad A_0, \qquad \tan\beta, \qquad \mathrm{sgn}(\mu), \tag{4}$$

the first three impose boundary conditions on the soft-SUSY breaking parameters at M_X, while the other two are boundary conditions at M_Z. Here M_0 is the universal, i.e. flavor independent, soft-breaking scalar mass. We thus have for example

$$m_{\tilde{\nu}_L} = m_{\tilde{\ell}_{L,R}} = m_{\tilde{q}_{L,R}} = m_{H_{1,2}} = M_0, \qquad @M_X, \tag{5}$$

where $m_{\tilde{\nu}_L}$ denotes the sneutrino mass, $m_{\tilde{\ell}_{L,R}}$ denote the $SU(2)$-doublet (L) and $SU(2)$ singlet (R) charged slepton masses, and $m_{\tilde{q}_{L,R}}$ denote the squark masses. $m_{H_{1,2}}$ are the soft-breaking Higgs boson masses. $M_{1/2}$ denotes the universal gaugino soft-breaking mass and we have for the bino (M_1), the $SU(2)$-wino (M_2) and the gluino mass (M_3), respectively [30]

$$M_1 = M_2 = M_3 = M_{1/2}, \qquad @M_X. \tag{6}$$

A_0 is the soft-breaking universal trilinear scalar interaction [31]. $\tan\beta = \frac{v_2}{v_1}$ is the ratio of the vacuum expectation values of the two Higgs doublets $H_{1,2}$ and $\mathrm{sgn}(\mu)$ is the sign of the Higgs mixing parameter of Eq. (2). The absolute value of μ as well as a possible bilinear scalar interaction B_0 are fixed by the electroweak symmetry breaking conditions at the SUSY breaking scale [29].

Given the five parameters in Eq. (4), we can compute the full supersymmetric spectrum and couplings at the electroweak scale through the renormalization group equations (RGEs). This has been studied in great detail [12–14]. An example spectrum is shown in Fig. 1 for the SPS1a parameter set [$M_0 = 100$ GeV, $M_{1/2} = 250$ GeV, $A_0 = -100$ GeV, $\tan\beta = 10$, $\mathrm{sgn} = (\mu) = +1$] [17]. In the left column (red), we have the neutral scalars ($h^0, H^0, A^0, \tilde{\nu}_{Li}$) as well as the charged Higgs bosons ($H^\pm$). In the second column (black), we have the charged slepton masses. In the third column (light blue), we show the neutralinos ($\tilde{\chi}^0_{i=1,2,3,4}$) and charginos ($\tilde{\chi}^\pm_{1,2}$) and in the fourth column (marine blue) the squarks ($\tilde{u}$, $\tilde{d}$, $\tilde{c}$, $\tilde{s}$, $\tilde{t}$, $\tilde{b}$) and gluinos $\tilde{g}$.

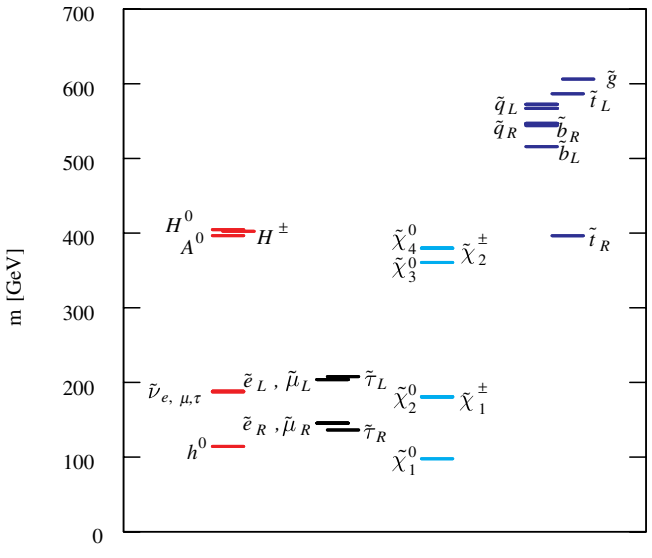

FIG. 1 (color online). The SPS1a supersymmetric spectrum. The P_6-mSUGRA parameter values are $M_0 = 100$ GeV, $M_{1/2} = 250$ GeV, $A_0 = -100$ GeV, $\tan\beta = 10$, $\mathrm{sgn}(\mu) = +1$. The up, down, charm and strange squarks are quasidegenerate in mass and are labeled by $\tilde{q}_{L,R}$.

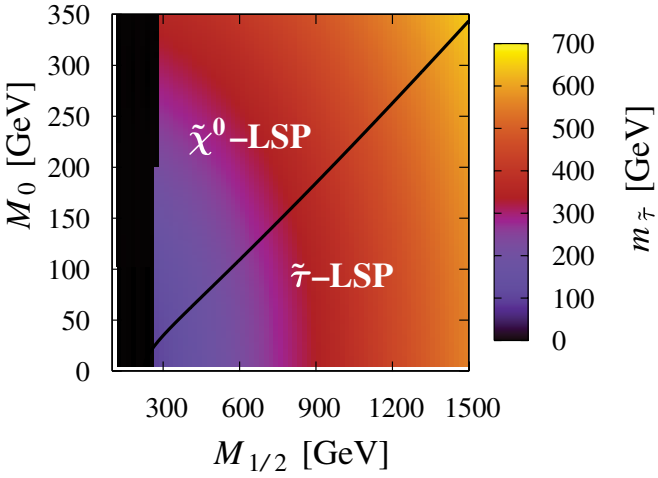

FIG. 2 (color online). Parameter space around SPS1a. The bar on the right displays the lightest stau mass. $A_0 = -100$ GeV, $\tan\beta = 10$, $\mathrm{sgn}(\mu) = +1$. The blackened out region to the left is excluded due to the LEP bounds and tachyons. The black contour distinguishes between areas with $\tilde{\chi}^0$-LSP and $\tilde{\tau}$-LSP.

We next discuss some typical features of this spectrum. First, the lightest supersymmetric particle (LSP) is the lightest neutralino. The SPS1a parameter values have been specifically chosen to ensure this. Since the LSP is stable in the P_6-MSSM, it must be electrically and color neutral for cosmological reasons [32], and a stable sneutrino LSP is experimentally excluded [33]. In P_6-mSUGRA, the regions of parameter space where the $\tilde{\chi}^0_1$ is not the LSP are thus excluded from further consideration. This is important for what follows since in $\not{P}_6$-mSUGRA this region is reopened. In Fig. 2, we have plotted the nature of the LSP in the M_0-$M_{1/2}$ plane around the SPS1a point. Most of the $\tilde{\chi}^0$-LSP parameter space leads to dark matter relic densities that are too high compared with the WMAP3 constraints if P_6 is conserved. Since we will consider the $\not{P}_6$ case where the LSP decays and does not constitute dark matter, we do not plot the constraint on Fig. 2. The blackened out region at smaller values of $M_{1/2}$ is excluded due to the LEP2 Higgs exclusion bound of $m_h > 114.4$ GeV at 95% C.L. [34], and/or the requirement of the absence of tachyons in order to obtain a valid electroweak vacuum. Note that, anticipating a 3 GeV error in SOFTSUSY's prediction of m_h, we have imposed a lower bound of 111.4 GeV in the figure. In large regions of parameter space the $\tilde{\chi}^0_1$ is indeed the LSP. Separated from this by the black contour, for low values of M_0 and large values of $M_{1/2}$ the lightest $\tilde{\tau}$ is the LSP. For later use, we also display the stau mass in the figure.

Second, in Fig. 1 it can be seen that the squarks and gluinos have masses much larger than M_0 and are much heavier than the sneutrinos and charged sleptons. This is because the strong interaction dominates the RGE running of the former. For $M_0 \gg M_{1/2}$ the slepton masses can be of order the squark and gluino masses, cf. SPS2 [17]. Third, one stop, the one which is predominantly $\tilde{t}_R$, is significantly lighter than the other squarks since the stop mixing $\sin\theta_t$ is of order m_t/M_{SUSY}, whereas M_{SUSY} is the SUSY breaking scale. Similarly the stau, which is dominantly $\tilde{\tau}_R$, is the lightest charged slepton, although the relative effect is much smaller, since $m_\tau \ll M_0$. Since the sleptons themselves are relatively light the $\tilde{\tau}_R$ is the next-to-lightest supersymmetric particle (NLSP). Fourth, the lightest Higgs boson is significantly lighter than the other Higgs bosons.

For SPS1a and other typical mSUGRA points the largest supersymmetric production cross sections at the LHC are for gluinos and squarks [35]. Usually, squarks and gluinos cascade decay via intermediate SUSY states to the LSP, leading eventually to a large missing p_T signature of the P_6-SSM.

In order to prepare for the LHC, it is important, given a supersymmetric spectrum, to analyze the resulting production processes and decays in great detail. In particular, this involves the full detector simulation for each signature. Even with the highly reduced parameter space of P_6-mSUGRA, this is beyond present capabilities. There is a special mSUGRA model with even fewer parameters: the so-called no-scale supergravity model [36], where we have as additional conditions

$$A_0 = M_0 = 0, \qquad @M_X. \tag{7}$$

This is however experimentally excluded through a combination of the LEP Higgs and chargino search [34] and the requirement of a neutral LSP. On the other hand, in the $\not{P}_6$-SSM the LSP need not be neutral and regions of no-scale mSUGRA parameter space are allowed [37].

III. THE P_6-VIOLATING MSSM

We next investigate the mass spectrum of the $\not{P}_6$-MSSM with particular focus on phenomenological analyses in preparation for the LHC. The superpotential is given in Eqs. (1)–(3) and has 48 additional parameters, λ_{ijk}, λ'_{ijk}, λ''_{ijk}, κ_i, with further parameters when we include SUSY breaking. Again, this parameter space is too large for a detailed phenomenological analysis and we restrict ourselves to the simplification of minimal supergravity with universal soft-SUSY breaking parameters at M_X. The $\not{P}_6$-mSUGRA model was developed in Refs. [37–40]. The RGEs connecting M_X with the weak scale are given at one-loop in Refs. [37,39–41]. The two-loop RGEs for the SM gauge couplings and the superpotential parameters [40] can have a qualitative impact on gauge coupling and b-τ unification and are included in our analysis. The impact of three-loop RGE terms is usually 1–2% [42] for the squarks, and negligible for weakly interacting sparticles. The two-loop RGEs for the soft-breaking terms have recently been calculated [43]. We restrict ourselves to one-loop RGEs for the soft-breaking parameters in order to perform scans in parameter space in a reasonably small amount of CPU-time. This is likely to be an excellent approximation for $\not{P}_6$ couplings $\lesssim 0.1$.

In order to keep the parameter space manageable, we shall also only consider one nonzero parameter of $W_{\not{P}_6}$ at a time at M_X. However, we include the possible dynamical generation of the other parameters through the coupled RGEs [37]. Note that at any given scale, the κ_i can be rotated away through a redefinition of the fields L_i, H_1 [37,44,45]. Within the context of supergravity with universal SUSY breaking we find it natural to rotate the κ_i to 0 at M_X [37]. Nonzero κ_i are then dynamically generated through the RGEs, leading to naturally small neutrino masses [37,38,40,46] in agreement with observations [47]. The parameters of $\not{P}_6$-mSUGRA are thus given by

$$M_0, M_{1/2}, A_0, \tan\beta, \mathrm{sgn}(\mu), \mathbf{\Lambda} \qquad @M_X, \quad \text{where } \mathbf{\Lambda} \in \{\lambda_{ijk}, \lambda'_{ijk}, \lambda''_{ijk}\}, \tag{8}$$

and we emphasize that in any given model only *one* nonzero parameter for $\mathbf{\Lambda}$ is chosen at M_X. In the no-scale mSUGRA case, although $M_0 = A_0 = 0$ at M_{GUT}, they are nonzero at the weak scale through the RGE running.

Given the additional couplings in $W_{\not{P}_6}$ as well as the corresponding soft-SUSY breaking terms, we have the following changes in the phenomenology compared to P_6-mSUGRA.

(1) Through the additional $\not{P}_6$ couplings the RGEs change and thus the spectrum and couplings change at low-energy [37,43].

(2) For $\not{P}_6$ the LSP is unstable and the cosmological bound [32] no longer applies. Thus any supersymmetric particle can be the LSP

$$\mathrm{LSP} \in \{\tilde{\nu}_L, \tilde{\ell}^{\pm}_{L,R}, \tilde{q}_{L,R}, \tilde{\chi}^0_1, \tilde{\chi}^{\pm}_1, \tilde{g}\}. \tag{9}$$

Within the $\not{P}_6$-mSUGRA model the nature of the LSP is determined through the initial conditions at M_X, Eq. (8), and the RGEs.

(3) Through the $W_{\not{P}_6}$-couplings, sparticles can be singly produced at colliders [48], e.g. resonant slepton production at hadron colliders [49].

(4) Because of the possible changes in the spectrum as well as the additional interactions, the decay patterns of the supersymmetric particles can change, see, for example, Ref. [50].

It is the purpose of this paper to investigate points 1 and 2 in detail. Points 3 and 4 will be exemplified in benchmark points later, but their detailed study will be left for later work. First we review the experimental bounds on the couplings $\mathbf{\Lambda}$, and consider experimentally excluded regions of parameter space.

A. Bounds on the Λ couplings

The low-energy 2σ bounds on the trilinear $\not{P}_6$-couplings are summarized in Refs. [7,51,52]. In Table I we show the largest allowed coupling in the five "classes" of couplings for scalar masses of 100 GeV. We do not include bounds which depend strongly on assumptions about quark mixing, such as those from RGE-induced neutrino masses, but rather those which come from more direct sources listed in Ref. [52]. The bounds shown are to be applied at M_Z, and no assumption about the high energy completion of the model has been made. We see that the weakest λ''_{ijk} bounds are not constraining with only perturbativity as a limiting effect (< 3.5 by some definitions). It should be noted that three of the λ'' couplings involving the first two generations have quite severe bounds [52]. The weakest λ'_{ijk} bounds also appear to allow large $\sim\mathcal{O}(1)$ couplings, but in fact many of the bounds are at the 10^{-1} level. Finally, the λ_{ijk} bounds are all around $5 \cdot 10^{-2}$.

However, within the context of a supergravity model formulated at the unification scale, we must take into account the $\not{P}_6$-RGEs. Considering the effect of the gauge couplings on the running of an individual $\mathbf{\Lambda}$ strengthens the bounds by a factor $\sim(1.5, 3.5, 4.3)$ at M_X for the couplings

TABLE I. Weakest 2σ direct bound on the five classes of couplings from low-energy processes such as a measurement of the Fermi constant in muon decay. Most of the bounds scale with $(\tilde{m}/100)$ GeV, where $\tilde{m}$ is the relevant scalar fermion mass for the process leading to the bound. "pert." indicates that the weakest bound only comes from perturbativity of the coupling $\mathcal{O}(1)$. Only one nonzero $\not{P}_6$ coupling at a time is considered.

λ_{ijk}	λ'_{1jk}	λ'_{2jk}	λ'_{3jk}	λ''_{ijk}
0.07	0.28	0.56	0.52	pert.

TABLE II. Weakest bound at M_X on the four classes of lepton-number violating couplings from the RGE generated κ_i for SPS1a. The superscript x denotes cases where there is no neutrino mass bound on some couplings in that class and so we have indicated the bound coming from the lack of tachyons. In the case of λ couplings the weakest bound arising from the RGEs is $\lambda_{231} < 0.55^x$ from the lack of tachyons [52]. We have instead included the translation of the weak scale bound to M_X. The weak-scale bound scales with the slepton mass ($m_{\tilde{\ell}}/100$ GeV) and is stronger than the tachyon bounds for slepton masses below the TeV scale.

	λ_{ijk}	λ'_{1jk}	λ'_{2jk}	λ'_{3jk}
d-mixing	0.046	$9.1 \cdot 10^{-4}$	$9.1 \cdot 10^{-4}$	$9.0 \cdot 10^{-4}$
u-mixing	0.046	0.15^x	0.15^x	0.15^x

(λ, λ', λ''), respectively [39,52]. The RGEs for the $\mathbf{\Lambda}$'s are highly coupled. In particular, the phenomenological requirement of $\mu \neq 0$ together with some λ or $\lambda' \neq 0$ at M_X leads to nonzero κ_i at the electroweak scale [37,40,46]. Through mixing of the neutrinos with the neutralinos, $\kappa_i \neq 0$ implies a nonzero neutrino mass [44]. Applying the cosmological bound on the neutrino mass, the resulting upper bounds on the $\lambda_{ijk}(M_X)$, $\lambda'_{ijk}(M_X)$ were obtained in Ref. [37]. The corresponding weakest bounds at M_X on the four classes of couplings are shown in Table II for the SPS1a point. Here, we have updated the bounds using the latest SOFTSUSY version [53]. Where the neutrino mass bound is not constraining, there is an upper bound coming from the nongeneration of negative mass squared scalars via RGE effects. Such "tachyon" bounds are denoted by a superscript "x" in the table. Most of the bounds strongly depend on the origin of CKM mixing in the SM quark sector [52,54]. We see from the table that if the CKM mixing originates solely in the down-quark sector we obtain much stricter bounds than solely up-quark sector mixing. The nature of the bounds within the supergravity context is important for models of flavor formulated at the GUT scale [45].

IV. BOUNDS ON $\not{P}_6$ NO-SCALE SUPERGRAVITY PARAMETER SPACE

Having discussed the bounds on the $\mathbf{\Lambda}$ couplings we next consider the constraints on $\not{P}_6$-mSUGRA parameter space arising from precision measurements. Specifically, we consider the anomalous magnetic moment of the muon $(g-2)$, the branching ratio $\mathrm{Br}(b \to s\gamma)$, and the branching ratio $\mathrm{Br}(B_s \to \mu^+\mu^-)$. We also briefly discuss the impact of the LEP Higgs mass bound.

All of the numerical calculations in the present paper have been performed using an unpublished $\not{P}_6$ version of SOFTSUSY [53]. The predictions for the P_6 conserving $\mathrm{Br}_{\mathrm{P}_6}(B_s \to \mu^+\mu^-)$, $(g-2)_\mu$, and $\mathrm{Br}_{\mathrm{P}_6}(b \to s\gamma)$ are calculated using MICROMEGAS 1.3.6 [55]. Throughout this paper, we use the default inputs $M_Z = 91.1875$ GeV and

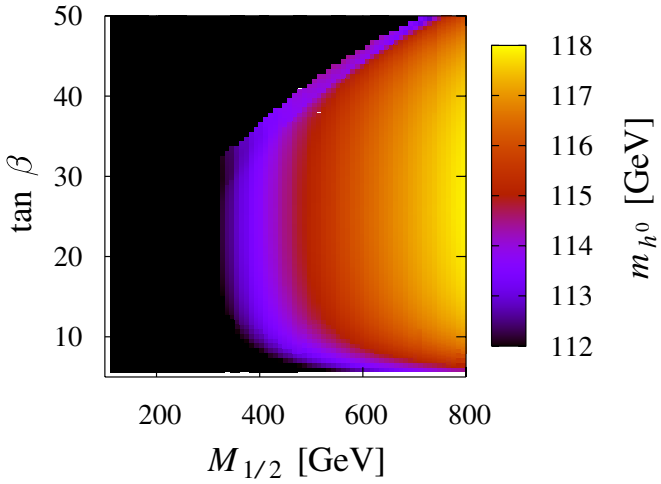

FIG. 3 (color online). Mass of h^0 in no-scale mSUGRA parameter space. The blacked out region corresponds to points that fail negative LEP2 Higgs constraints or that possess tachyonic scalars.

$m_t = 172.5$ GeV for the pole masses of the Z^0 boson and top quark, respectively. The weak-scale gauge couplings are set to their central values in the $\overline{MS}$ scheme $\alpha^{-1}(M_Z) = 127.918$, $\alpha_s(M_Z) = 0.1187$. Light quark masses are also set to their central values in the $\overline{MS}$ scheme: $m_b(m_b) = 4.25$ GeV, $m_u(2\text{ GeV}) = 0.003$ GeV, $m_d(2\text{ GeV}) = 0.00675$ GeV, $m_s(2\text{ GeV}) = 0.1175$ GeV and $m_c(m_c) = 1.2$ GeV [56].

The prediction for the lightest CP-even Higgs mass, m_h, is shown in Fig. 3 as a function of the no-scale mSUGRA parameter space. As discussed above, a lower bound of 111.4 GeV is imposed upon SOFTSUSY's prediction of m_h. We find $m_h < 124$ GeV for values of $M_{1/2} < 1500$ GeV.

A. The muon $(g-2)$ value

The anomalous magnetic moment of positively and negatively charged muons is one of the very few predictions of the SM that are *not* in good accordance with experiment. The combined experimental measurement is [57]

$$a_\mu^{\mathrm{exp}} \equiv \frac{(g-2)_\mu}{2} = 116\,592\,08.0(6.3) \times 10^{-10}. \quad (10)$$

The SM prediction requires the input of data on hadronic spectral functions. There is a well-known discrepancy between the predictions based on data from $e^+e^- \to$ hadrons ("e^+e^--based") and those based on semileptonic tau decays ("tau-based") [58]. Following the particle data group [59], we focus on the e^+e^--based predictions and obtain

$$\delta a_\mu \equiv a_\mu^{\mathrm{exp}} - a_\mu^{\mathrm{SM}} = (22.2 \pm 10.2) \times 10^{-10}, \quad (11)$$

where all theoretical and experimental errors have been added in quadrature. δa_μ is smaller and within one sigma

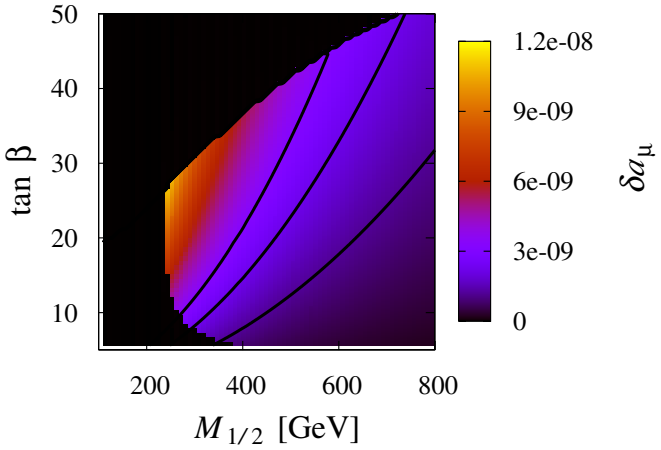

FIG. 4 (color online). No-scale P_6 contribution to $\delta a_\mu^{\text{SUSY-th}}$, i.e. $M_0 = A_0 = 0$ at M_X. The blacked out region to the left and upper left is excluded due to LEP exclusion bounds and tachyons. The black contours show the region of parameter space that is consistent with the empirical central value of $g-2$, plus or minus 1σ.

from zero when the τ-based prediction is used. We shall constrain the $\not{P}_6$-MSSM such that the predicted $\delta a_\mu^{\text{SUSY}} \equiv a_\mu^{\text{exp}} - a_\mu^{\text{SUSY-th}}$ provides the missing component of $(g-2)_\mu$ in Eq. (11).

In order to compute $\delta a_\mu^{\text{SUSY-th}}$, we use MICROMEGAS 1.3.6 [55] for the one-loop supersymmetric P_6 part, which can be enhanced by $\tan\beta$. The one-loop $\not{P}_6$ contribution is of order

$$(\delta a_\mu)^{\not{P}_6} \sim \mathcal{O}\left(\frac{m_\mu^2 |\mathbf{\Lambda}|^2}{32\pi^2 \tilde{m}^2}\right), \tag{12}$$

for $\mathbf{\Lambda} \in \{\lambda_{ijk}, \lambda'_{ijk}\}$ [60], where $\tilde{m}$ is a sparticle mass that appears in the loop. For $\tilde{m} > 300$ GeV and $|\mathbf{\Lambda}|^2 < 0.1$ (as is the case for the points studied here), $(\delta a_\mu)^{\not{P}_6} < \mathcal{O}(10^{-11})$ and so we neglect it, taking the P_6 contribution only.

Fig. (4) shows the allowed region of $\delta a_\mu^{\text{SUSY-th}}$ in the no-scale MSSM in the $M_{1/2}$-$\tan\beta$-plane as the region between the contours. At higher SUSY masses (higher $M_{1/2}$), $\delta a_\mu^{\text{SUSY-th}}$ becomes smaller as the SUSY contributions decouple due to mass suppression of sparticle propagators in the one-loop diagrams. Here, the prediction of a_μ is similar to that of the SM. δa_μ increases for higher $\tan\beta$, which is why the contours move to the right with increasing $\tan\beta$.

B. Br($b \to s\gamma$)

Next we consider the measurement of Br($b \to s\gamma$). The current experimental result is [61]

$$\text{Br}(b \to s\gamma)_{\text{exp}} = (3.55 \pm 0.26) \times 10^{-4}, \tag{13}$$

where we have added the statistical and systematic errors in quadrature, including the uncertainty for the shape function of the photon energy spectrum. If we now include a combined theoretical error of 0.30×10^{-4} [62] and add it in quadrature to the experimental error we obtain the allowed range for the central theoretical value at the 2σ level [63]

$$2.76 \times 10^{-4} < \text{Br}(b \to s\gamma)_{\text{th}} < 4.34 \times 10^{-4}. \tag{14}$$

The P_6-MSSM branching ratio is plotted in Fig. (5) for the no-scale mSUGRA model. Again, $M_{1/2}$ and $\tan\beta$ are varied. The contour shows the midvalue of Br($b \to s\gamma$), i.e. 3.55×10^{-4}.

The P_6 conserving contribution to Br($b \to s\gamma$) of the no-scale mSUGRA model is thus in agreement with the experimental bounds at 2σ in almost the entire plotted region. An estimate for the $\not{P}_6$ contribution to this process is given in Ref. [41]. There are many potential contributions from products of two different $\mathbf{\Lambda}$ couplings. Although we assume only one nonzero $\mathbf{\Lambda}$ coupling at the GUT scale, several different couplings are generated by the RGE evolution to the weak scale providing a nonzero $\not{P}_6$ contribution. However, the couplings generated by the RGEs are suppressed by loop factors such that the $\not{P}_6$ generated contribution to Br($b \to s\gamma$) is also highly suppressed. We have generalized Ref. [41] to include CKM quark mixing and explicitly checked that the contribution to Br($b \to s\gamma$) is less than 10^{-6} in every case studied and therefore negligible. For example, the difference between the predicted values of Br($b \to s\gamma$) in the P_6 case and the combined P_6 and $\not{P}_6$ case for the no-scale mSUGRA point $M_{1/2} = 400$ GeV, $\tan\beta = 20$ is always smaller in magnitude than 10^{-9} for quark mixing purely in the down sector and for any λ'_{ijk} set at its upper limit. A similar conclusion holds in the case of up-mixing.

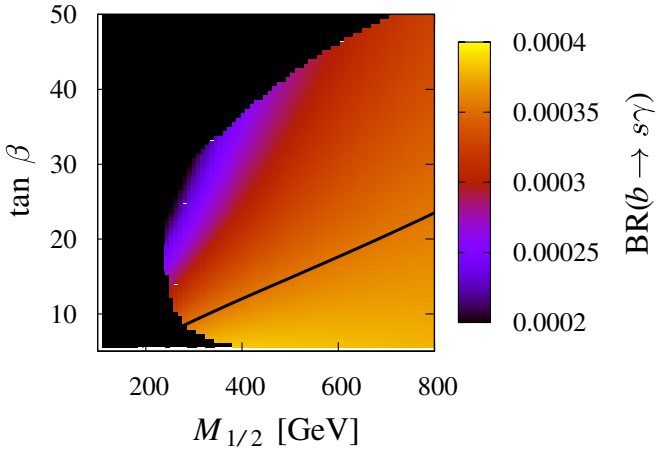

FIG. 5 (color online). P_6-MSSM no-scale mSUGRA contribution to Br($b \to s\gamma$). The blackened out region is excluded due to LEP measurements and the existence of tachyons. The contour shows the midvalue of Br($b \to s\gamma$).

C. Br($B_s \to \mu^+\mu^-$)

The Tevatron experiments have recently tightened the upper limit on the rare decay branching ratio Br($B_s \to \mu^+\mu^-$), currently the best CDF bound is [64]

$$\mathrm{Br}_{\mathrm{exp}}(B_s \to \mu^+\mu^-) < 1 \times 10^{-7} \tag{15}$$

at the 95% C.L. The SM prediction is [65]:

$$\mathrm{Br}_{\mathrm{SM}}(B_s \to \mu^+\mu^-) = (3.35 \pm 0.32) \times 10^{-10}. \tag{16}$$

In the P_6-MSSM, the branching ratio can be significantly larger than in the SM since it is proportional to $(\tan\beta)^6/M_A^4$ [66,67]. The $\tan\beta$ enhancement comes from the dependence on bottom and muon Yukawa couplings. The above experimental bound, Eq. (15), constrains some of the $M_0 \neq 0$ mSUGRA parameter space [68]. In Fig. (6) we show the P_6-mSUGRA prediction for Br($B_s \to \mu^+\mu^-$) for the specific parameter range of the *no-scale* mSUGRA model, i.e. with $M_0 = 0$, as a function of $M_{1/2}$ and $\tan\beta$. We see that in this case, it is at least an order of magnitude below the experimental bound over the whole plane.

Since the P_6-mSUGRA contribution is small, we look at the $\not{P}_6$ contribution alone, i.e. without interference with the SM or P_6 conserving contribution. The $\not{P}_6$ contribution to Br($B_s \to \mu^+\mu^-$) was calculated in Ref. [69]. Here, we generalize the calculation in order to include the L-R-mixings of the mediating squarks and also allow for non-degenerate sparticle masses. The computation is presented in the appendix. We use this generalized result in an unpublished $\not{P}_6$ version of SOFTSUSY to give an estimate of the contribution to the decay rate. In the case of one dominant $\not{P}_6$ operator at the GUT scale, the contribution to Br($B_s \to \mu^+\mu^-$) is always less than 10^{-14} once the $\mathbf{\Lambda}$ have been bounded by experimental constraints, irrespective of the nature of the CKM mixing. For our analysis, the $\not{P}_6$ contribution to Br($B_s \to \mu^+\mu^-$) is therefore neglected in the rest of the paper. However, we note that if we drop the requirement of only one nonzero GUT-scale $\mathbf{\Lambda}$ coupling, much larger $\not{P}_6$ contributions are possible. For example, choosing $\lambda_{122}(M_{\mathrm{GUT}}) = 6.3 \times 10^{-4}$ and $\lambda'_{132}(M_{\mathrm{GUT}}) = 7.6 \times 10^{-5}$ achieves a $\not{P}_6$ contribution to Br($B_s \to \mu^+\mu^-$) as high as 10^{-7}. The corresponding product bounds for weak-scale couplings are given in Ref. [69].

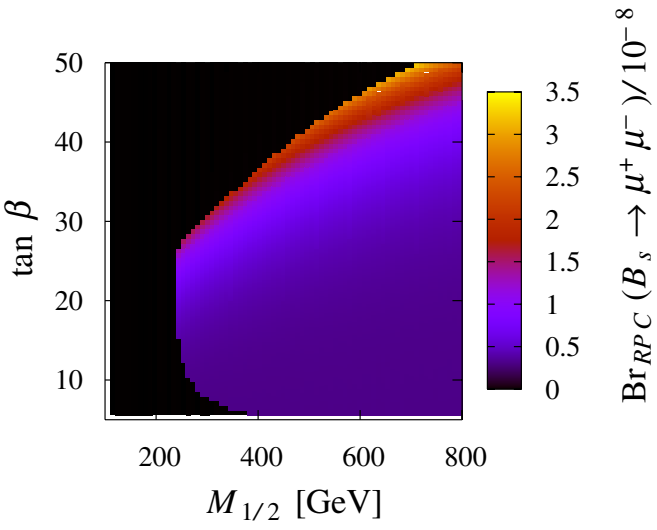

FIG. 6 (color online). P_6 contribution to $\mathrm{Br}_{\mathrm{SM}}(B_s \to \mu^+\mu^-)$ in no-scale mSUGRA. The blacked out region is excluded by LEP direct sparticle and Higgs searches, as well as the requirement of no tachyons.

V. $\not{P}_6$-SPECTRUM

In this section, we investigate the supersymmetric spectrum in the $\not{P}_6$-mSUGRA model, taking into account the constraints of the previous section. We are particularly interested in the nature of the LSP, which is of fundamental importance for the resulting collider signatures. However, we first investigate the overall shift in the supersymmetric spectra due to the $\mathbf{\Lambda}$ couplings. Finally, we study the changes in the mass ordering of sparticles. The latter determines the cascade decay patterns, which in turn are also essential for the collider signatures.

A. Shift in spectrum due to $\mathbf{\Lambda}$-RGEs

In order to determine the low-energy $\not{P}_6$ supersymmetric spectrum from the parameter set at M_X, Eq. (8), we must employ the $\not{P}_6$ RGEs [37,39–41]. They have been programmed at one-loop order in an unpublished version of SOFTSUSY [53]. The leading effect of the $\mathbf{\Lambda}$ couplings on the running of the supersymmetric masses is $\sim \mathcal{O}[\Lambda^2/(16\pi^2)\ln(M_{\mathrm{GUT}}/M_Z)]$. Given the bounds in Table II, in most cases we only expect small shifts in the spectrum in the mSUGRA scenario. In order to illustrate the effects, we choose as a comparison the low-energy spectrum of the SPS1a point [17] with conserved P_6. It is listed in the second column of Table III and also shown in Fig. 1. In the first column we have listed the supersymmetric particles.

In the remaining columns, we show various $\not{P}_6$ spectra resulting from one nonzero coupling at M_X and with the P_6 conserving parameters as for SPS1a. In the third column of Table III, we list the masses for the largest allowed $LL\bar{E}$ coupling: $\lambda_{123}(M_X) = 0.08$. We see that the maximal relative shift of any supersymmetric particle is about 2% and is in the $\tilde{e}_R$ mass. For most particles the shift is below 1%, which is indistinguishable from the P_6 spectrum at the level of significance we display. In the fourth column, we list the spectrum for $\lambda'_{331}(M_X) = 0.122$, i.e. the case of up-mixing [70]. Here we obtain significant shifts in the masses of $\tilde{\nu}_\tau$ and $\tilde{\tau}_{1,2}$, which directly couple to the operator $\lambda_{331}L_3Q_3\bar{D}_1$. In particular, this leads to the novel possibility of a tau sneutrino LSP, which we discuss in more detail below. There are also slight shifts in the $\tilde{d}_1$, $\tilde{b}_1$, $\tilde{t}_2$ masses, with the operators again coupling directly to the dominant

TABLE III. Low-energy supersymmetric spectra for the point SPS1a in the P_6 conserving case, column two, and in various maximum $\not{P}_6$ scenarios in columns 3–5. In the latter other than $\mathbf{\Lambda}(M_X)$ all SUSY parameters are as in SPS1a. The masses are given in GeV and we have highlighted in bold face those changes compared to the P_6-spectrum which are 5 GeV or more. In the case of λ'_{331}, we assume the entire CKM mixing is in the up-sector. In the case of λ''_{212} we have assumed the CKM mixing is in the down-sector.

	P_6	$\lambda_{123} = 0.08$	$\lambda'_{331} = 0.122$	$\lambda''_{212} = 0.5$
$\tilde{\nu}_e$	189	187	189	189
$\tilde{\nu}_\mu$	189	187	189	189
$\tilde{\nu}_\tau$	188	188	**93**	188
$\tilde{e}^{\pm}_{R,L}$	146; 206	146; 205	146; 206	146; 206
$\tilde{\mu}^{\pm}_{R,L}$	146; 206	146; 205	146; 206	146; 206
$\tilde{\tau}^{\pm}_{1,2}$	137; 210	134; 210	**104**; **159**	137; 210
$\tilde{u}_1$	552	552	552	552
$\tilde{u}_2$	567	567	567	568
$\tilde{c}_1$	552	552	552	**394**
$\tilde{c}_2$	567	567	567	**562**
$\tilde{d}_1$	552	552	**536**	**393**
$\tilde{d}_2$	575	575	574	**570**
$\tilde{s}_1$	552	552	552	**393**
$\tilde{s}_2$	575	575	575	**570**
$\tilde{b}_{1,2}$	518; 550	518; 550	**511**; 549	519; 551
$\tilde{t}_{1,2}$	400; 591	400; 591	399; **586**	401; 592
$\tilde{\chi}^0_1$	97	97	97	97
$\tilde{\chi}^0_2$	181	181	181	181
$\tilde{\chi}^0_3$	362	362	360	362
$\tilde{\chi}^0_4$	380	380	379	380
$\tilde{\chi}^{\pm}_1$	182	182	181	182
$\tilde{\chi}^{\pm}_2$	378	378	377	378
$\tilde{g}$	610	610	610	**604**
h^0	110	110	110	110
H^0	397	397	396	397
$H^{\pm}$	405	405	404	405
A^0	397	397	396	397

$\not{P}_6$ operator. In the case of down-mixing, λ'_{331} is bounded to be less than 10^{-3} and the spectrum is indistinguishable from the P_6 spectrum in the second column and we do not list it.

The λ'' couplings are not bounded by neutrino masses and in some cases can still be at the perturbativity limit. As an example, we choose $\lambda''_{212}(M_X) = 0.5$. We show the spectrum in the last column on the right. Here we obtain significant shifts ($\sim 30\%$) in the masses of $\tilde{c}_1$, $\tilde{d}_1$, $\tilde{s}_1$, which are all dominantly $SU(2)$ singlets and thus directly couple to the leading $\not{P}_6$ operator. There are also small shifts in the corresponding doublet masses as well as the gluino mass (originating from changes to the 1-loop threshold contributions from the squarks). We expect similar effects for the other large λ'' couplings, i.e. the fields which directly couple should experience the largest mass shifts.

B. Nature of the LSP

As pointed out in Eq. (9), in the $\not{P}_6$-MSSM in principle any supersymmetric particle can be the LSP. However, given the restricted parameter space of Eq. (8) at M_X, it is a computational question as to which LSPs are attained in a given model. In the general mSUGRA case and for vanishing $\mathbf{\Lambda}$-couplings, we have the well-known (but usually ignored) region shown in the lower right of Fig. 2, where the lightest stau ($\tilde{\tau}_1$) is the LSP. For $A_0 = -100$ GeV, $\tan\beta = 10$, $\mathrm{sgn}(\mu) = +1$ the black line denoting the border between the $\tilde{\chi}^0_1$-LSP region, at high values of M_0 and the $\tilde{\tau}_1$-LSP region at low values, is approximately given by

$$M_{1/2} = 3.8 \cdot M_0 + 175 \text{ GeV}. \tag{17}$$

Such a $\tilde{\tau}_1$-LSP region always exists in mSUGRA models, since for rising $M_{1/2}$ and fixed M_0 the gaugino masses grow more quickly than the slepton masses, see the approximate formulæ in Ref. [14]. However already for $M_0 \gtrsim 200$ GeV, we must have $M_{1/2} \gtrsim 1$ TeV for a stau LSP. We can read-off the no-scale case along the x axis in Fig. 2, where $M_0 = 0$. This always results in a $\tilde{\tau}_1$-LSP.

If we now turn on the $\mathbf{\Lambda}$-couplings, this picture is in principle modified [43]. However as seen in the previous section, for the maximally allowed couplings the shifts in the spectrum are typically modest for all but the λ''-couplings and exceptional cases of the λ'_{331} coupling. For SPS1a, the charged sleptons are the next lightest particles. Other than the stau, we thus might expect a $\tilde{\mu}_1$ LSP. However, we have checked that this requires λ_{ijk}- or λ'-couplings far exceeding the upper bounds given in Table II [53]. (The λ''-couplings do not significantly affect the sleptons, see Table III.) In fact, in the case of down-mixing in the weak-scale CKM matrix, we have found no further LSP. While the precise numerical bounds on the couplings are sfermion mass dependent and were only calculated for the SPS1a point [37], the qualitative conclusion regarding possible identities of the LSP holds in the region studied in Fig. 2.

The significant shifts in the spectrum in the λ''_{212} case mainly affect the squarks, but they are too small to obtain a squark LSP. However, for up-mixing in the case of nonzero $\lambda'_{331}(M_{\mathrm{GUT}})$, it is possible to obtain a tau sneutrino LSP. As can be seen in Fig. 7, for the very narrow region $\lambda'_{331} = 0.12$–0.14, a tau sneutrino LSP results at SPS1a. The lightest neutralino becomes the NNLSP for $\lambda'_{331} > 0.13$.

To summarize, we have found that there is a well-motivated region in the $\not{P}_6$ no-scale supergravity model where the $\tilde{\tau}_1$ is the LSP. This region has hitherto been almost completely ignored in the literature [37,71]. We have also found a very special region in parameter space where we have a tau sneutrino LSP, i.e. we have one of the central results of our paper

$$\text{LSP} \in \{\tilde{\chi}^0_1, \tilde{\tau}_1, \tilde{\nu}\}. \tag{18}$$

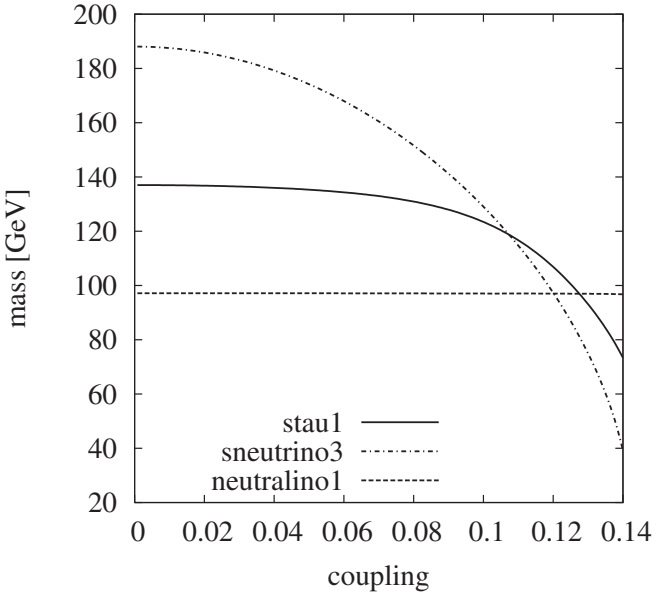

FIG. 7. LSP, NLSP and NNLSP at SPS1a for varying $\lambda'_{331}(M_{\rm GUT})$. All quark mixing has been placed in the up sector at the weak scale.

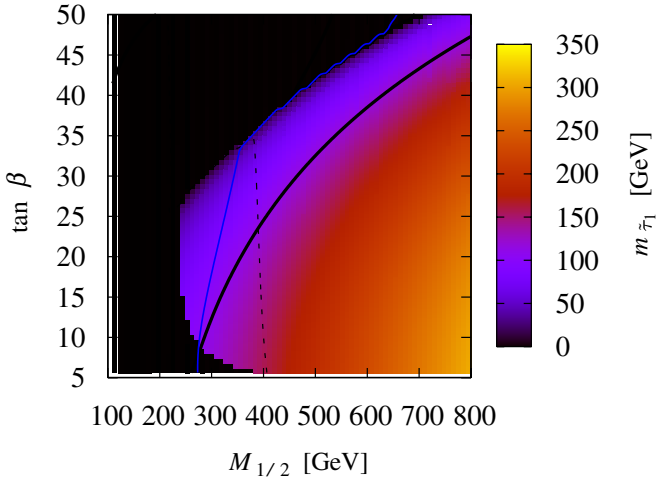

FIG. 8 (color online). Mass of the stau-LSP in the $M_{1/2}$-tanβ-plane for no-scale mSUGRA. The blackened out region is excluded due to LEP bounds and tachyons. The black contour shows $m_h = m_{\tilde{\tau}_1}$. The dashed contour shows $m_{\tilde{\chi}_1^0} = m_{\tilde{e}_1} \approx m_{\tilde{\mu}_1}$, thus separating regions of $\tilde{\chi}_1^0$ NLSP (left) and $\tilde{\chi}_1^0$ NNNLSP (right). The blue contour shows where $m_{\tilde{\chi}_2^0} = m_{\tilde{\tau}_2}$.

In the following, we investigate the spectrum in detail for the case of a stau or sneutrino LSP. We then propose several $\not{P}_6$ benchmark points for follow-up systematic phenomenological analyses, including detector simulations.

C. Mass ordering in the stau-LSP region

In the standard mSUGRA model, supersymmetric particles are produced in pairs at colliders. They then cascade decay to the neutralino LSP through various intermediate supersymmetric states. The LSP escapes detection, which results in the typical missing transverse energy signature for the P_6-MSSM.

We are here interested in the mSUGRA region with a $\tilde{\tau}_1$-LSP. If the $\mathbf{\Lambda}$ couplings are small, as indicated by most of the bounds, sparticles will be dominantly pair-produced in the usual P_6 conserving channels [72]. They will then cascade decay down to the lighter supersymmetric particles eventually ending at the $\tilde{\tau}_1$-LSP. The nature of these cascades and thus the final-state particles will be different from the P_6-case since the ordering of the spectrum can change. In particular, the lightest neutralino will be heavier than one or more supersymmetric particle. Finally, the resulting LSPs will decay into SM particles, the flavor content of which depends on the dominant $\mathbf{\Lambda}$ coupling and again on the sparticle mass ordering. We thus investigate in more detail the mass ordering.

Figure 8 shows the $\tilde{\tau}$-LSP mass in the $M_{1/2}$-tanβ-plane for no-scale mSUGRA with $\mathrm{sgn}(\mu) = +1$. We shall mainly focus on the case of lepton-number violating couplings. Here in the figure, the $\not{P}_6$-couplings are set to zero, which will be a good approximation for all cases where they are $\lesssim 0.05$. The blackened out region to the left is excluded due to the LEP2 Higgs search and the absence of tachyons. In the P_6 limit, LEP2 gave an 86 GeV lower bound on the lightest stau mass [56], which is also included.

The contours in the figure delineate regions differing in sparticle mass ordering. The black contour shows where the mass of the lightest CP-even Higgs, m_{h^0}, is equal to the mass of the $\tilde{\tau}_1$. For models where $M_{1/2}$ is smaller, i.e. to the left, $m_{h^0} > m_{\tilde{\tau}_1}$. The dashed contour shows the analogous effect for $m_{\tilde{\chi}_1^0} = m_{\tilde{e}_1}$, i.e. to the right the neutralino is heavier than the lightest selectron. The neutralino is then also heavier than the lightest smuon, since $m_{\tilde{\mu}_1} \approx m_{\tilde{e}_1}$, with the former slightly lighter. We thus have an extensive region, where $\tilde{\chi}_1^0$ is the fourth lightest supersymmetric particle, the NNNLSP. This should particularly have an impact on slepton pair production signatures. For squark pair production, the heavier neutralinos and the two charginos which can appear in the cascade decay can in principle have significant branching ratios, where they completely skip the lightest neutralino directly decaying to the light sleptons.

It is also worth pointing out that for high $M_{1/2}$ and high tanβ, we get the following additional changes compared to the SPS1a spectrum.

$$m_{\tilde{\chi}_2^0} > m_{\tilde{\tau}_2}, \tag{19}$$

$$m_{\tilde{\nu}_3} < m_{\tilde{\tau}_2} < m_{\tilde{\nu}_{1,2}}. \tag{20}$$

In summary, we expect a significantly changed phenome-

nology in the no-scale $\tilde{\tau}_1$-LSP parameter space, both compared to the P_6 case but also compared to the hitherto extensively studied $\not{P}_6$ case (so far usually called the R-parity violating case) with a neutralino LSP. In order to investigate this in more detail in the future, we propose several benchmarks which are representative of the possible collider signatures.

VI. $\not{P}_6$-BENCHMARKS

We now turn to the description of the $\not{P}_6$-mSUGRA benchmarks. In order to fully specify the model, we must fix both the standard mSUGRA parameters: $M_{1/2}$, M_0, A_0, $\tan\beta$, $\mathrm{sgn}(\mu)$ as well as the $\mathbf{\Lambda}$ couplings. We first discuss the spectra of the benchmark points and then go on to detail sparticle decays.

A. Sparticle spectra

The first no-scale mSUGRA parameter set consists of a rather light sparticle spectrum: $M_{1/2} = 400$ GeV, $\tan\beta = 13$ and $\mathrm{sgn}(\mu) = +1$. The spectrum is shown in Fig. 9. As can be seen by a comparison with Fig. 1, the spectrum is similar to SPS1a. The most important difference is a $\tilde{\tau}$-LSP of mass 148.2 GeV. The selectron and smuon are the next lightest sparticles, with masses 160.8 and 161.3 GeV, respectively. The lightest neutralino is the NNNLSP with a mass 161.5 GeV, almost degenerate with the lightest charged sleptons, such that the direct decays are suppressed. The sparticles are light so that there should be copious SUSY particle production at the LHC. We have calculated this spectrum in the limit of zero $\mathbf{\Lambda}$ and the spectrum in Fig. 9 will be a good approximation when all $\mathbf{\Lambda} \ll 1$, as is the case for two of our benchmarks to be specified below: BC1 and BC2.

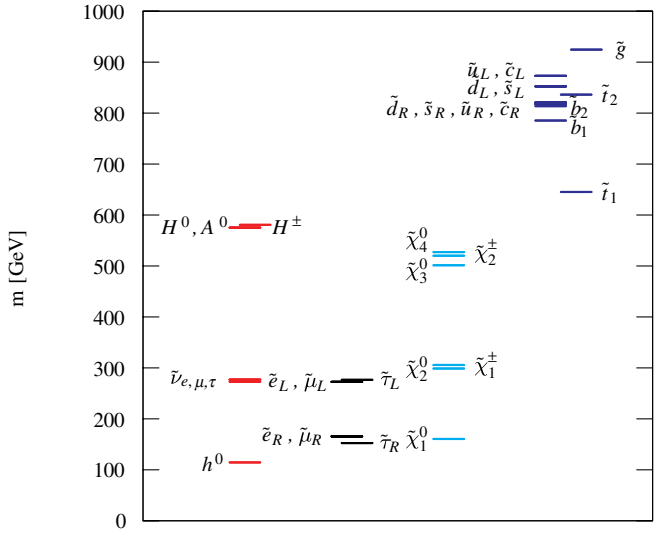

FIG. 9 (color online). Sparticle spectrum for no-scale mSUGRA parameter set: $M_{1/2} = 400$ GeV, $\tan\beta = 13$, $\mathrm{sgn}(\mu) = +1$, and $\Lambda = 0$.

For the next set of input parameters, we pick a point from Fig. 7 with an SPS1a-like spectrum but with a tau sneutrino LSP, in order to obtain different signatures, i.e. here we *must* choose a nonzero $\mathbf{\Lambda}$: $\lambda'_{331}(M_{\mathrm{GUT}}) = 0.122$, $\tan\beta = 10$, $M_0 = 100$ GeV, $M_{1/2} = 250$ GeV, $A_0 = -100$ GeV, $\mathrm{sgn}(\mu) = +1$ and the weak-scale quark mixing is solely in the up sector. The spectrum is displayed in Fig. 10. Numerically it is given in Table III. The mass ordering of the lightest sparticles is $m_{\tilde{\tau}_1} > m_{\tilde{\chi}_1^0} > m_{\tilde{\nu}_\tau}$. The spectrum is light and would lead to copious SUSY production at the LHC.

The final no-scale mSUGRA parameter set consists of a somewhat heavier spectrum: $M_{1/2} = 600$ GeV, $\tan\beta = 30$, and $\mathrm{sgn}(\mu) = +1$, $\lambda''_{212}(M_{\mathrm{GUT}}) = 0.5$. The spectrum is displayed in Fig. 11; note the scale difference to Fig. 9. "SUSY" detection and measurement at this point will be more difficult than for the no-scale set I, but still easily possible [5]. We have chosen this point to represent the novel mass ordering where the neutralino is the NNNLSP, as discussed in the previous section: $m_{\tilde{\chi}_1^0} > m_{\tilde{e}_R,\tilde{\mu}_R} > m_{\tilde{\tau}_R}$.

B. Sparticle decays

As pointed out in Ref. [37], depending upon the flavor structure of the $\mathbf{\Lambda}$ couplings, the non-neutralino LSP may dominantly undergo 2 or 4-body decays. Since we expect two LSPs per SUSY event, the 4-body decays will significantly change the number of particles in the final state and

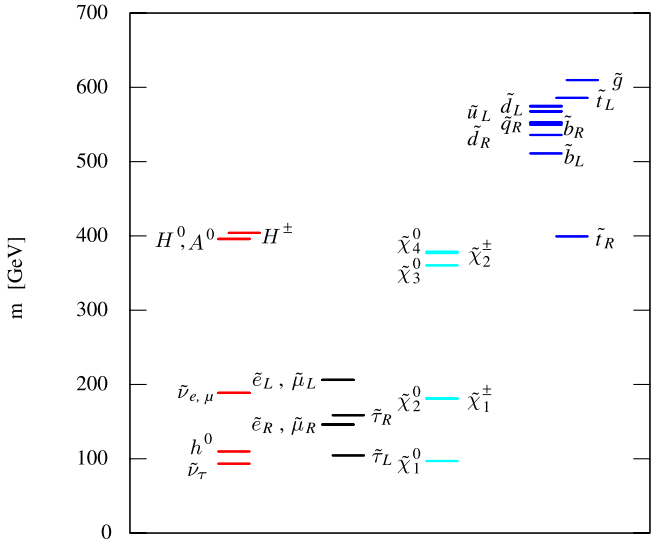

FIG. 10 (color online). Sparticle spectrum for mSUGRA parameter set with a sneutrino LSP: $\lambda'_{331}(M_{\mathrm{GUT}}) = 0.122$, $\tan\beta = 10$, $M_0 = 100$ GeV, $M_{1/2} = 250$ GeV, $A_0 = -100$ GeV, $\mathrm{sgn}(\mu) = +1$ and the weak-scale quark mixing is solely in the up sector. Numerically the spectrum is given in Table III. We have omitted $\tilde{s}_L$, $\tilde{c}_L$ which are almost degenerate with $\tilde{d}_L$, $\tilde{u}_L$ respectively. We have combined $\tilde{u}_R$, $\tilde{c}_R$, $\tilde{s}_R$ into $\tilde{q}_R$.

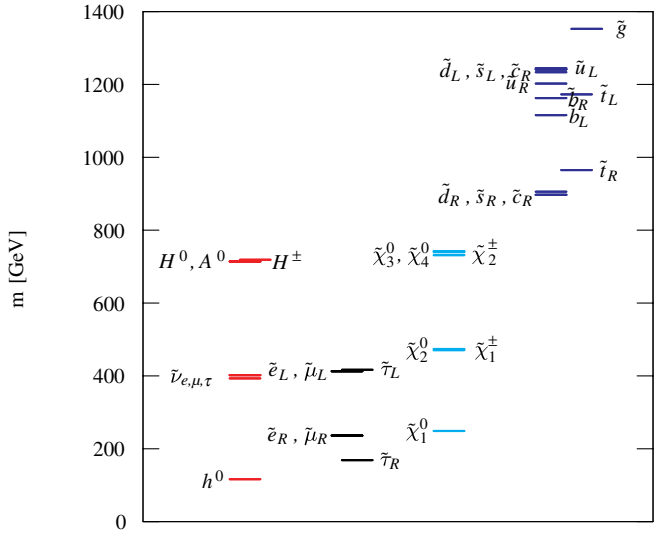

FIG. 11 (color online). Sparticle spectrum for no-scale mSUGRA parameter set: $M_{1/2} = 600$ GeV, $\tan\beta = 30$, $\mathrm{sgn}(\mu) = +1$, $\lambda''_{212}(M_{\mathrm{GUT}}) = 0.5$.

therefore alter the potential signatures. A benchmark where 2-body LSP decays dominate and another where 4-body LSP decays dominate then seems expedient. We choose a stau LSP for the 4-body decay, since the calculations for the partial widths have been completed [73] and the sneutrino has no 4-body decays. We choose a point with a tau sneutrino LSP, which necessarily has 2-body decays because of the dominant λ'_{331} coupling, which it directly couples to.

For small $\mathbf{\Lambda}$, the LSP may be long-lived, leading to sparticles with a measurable detached decay vertex in the detector. If the $\not{P}_6$ couplings are even smaller, such decays are longer lived than $\sim 10^{-6}$ seconds, the staus will decay outside of the detector and appear as heavily ionizing tracks. This possibility has been examined recently in the literature [74], albeit in a different context. In an intermediate $\not{P}_6$ coupling regime, significant numbers of the staus will decay in the detector providing heavily ionising tracks with detached vertices. This possibility is new and interesting and so we shall include a benchmark that covers it.

We note in passing that the case of a long-lived LSP in principle also include timescales which are relevant for cosmology, i.e. $\tau(\mathrm{LSP}) > \mathcal{O}(1\ \mathrm{sec})$ and the resulting bounds must be taken into account [75]. As we saw, in the case of R-parity violation, in principle any supersymmetric particle can be the LSP. We found in our restricted mSUGRA scenarios either a neutralino, a sneutrino or a stau LSP. As has been recently investigated in some detail the cosmological bounds on a long-lived charged particle for example from nucleosynthesis are very different for charged [76–79] and neutral particles [75,76,80–84]. For example the long-lived charged particles can form bound states with the free nuclei thus affecting their nuclear reactions, which in turn directly affects the abundance of the light elements [78]. A more detailed analysis is unfortunately beyond the scope of this paper.

λ''_{ijk} couplings necessarily lead to 4-body stau decays. These involve many jets in the final state as well as taus from the $\tilde{\tau}$ decays. Thus the fourth benchmark shall have a nonzero λ''_{ijk} at M_{GUT}. More precisely, the four benchmarks chosen are

(i) *BC1*: no-scale mSUGRA with $\lambda_{121}(M_{\mathrm{GUT}}) = 0.032$, $\tan\beta = 13$, $M_{1/2} = 400$ GeV, $\mathrm{sgn}(\mu) = +1$. The spectrum is shown in Fig. 9.

(ii) *BC2*: no-scale mSUGRA with $\lambda'_{311}(M_{\mathrm{GUT}}) = 3.5 \times 10^{-7}$, $\tan\beta = 13$, $M_{1/2} = 400$ GeV, $\mathrm{sgn}(\mu) = +1$. The spectrum is shown in Fig. 9. The LSP is long-lived.

(iii) *BC3*: mSUGRA with $\lambda'_{331}(M_{\mathrm{GUT}}) = 0.122$, $\tan\beta = 10$, $M_0 = 100$ GeV, $M_{1/2} = 250$ GeV, $A_0 = -100$ GeV, $\mathrm{sgn}(\mu) = +1$ and weak-scale quark mixing solely in the up sector. The spectrum is shown in Fig. 10 and given in Table III.

(iv) *BC4*: no-scale mSUGRA with $\lambda''_{212}(M_{\mathrm{GUT}}) = 0.5$, $\tan\beta = 30$, $M_{1/2} = 600$ GeV, $\mathrm{sgn}(\mu) = +1$. The spectrum is shown in Fig. 11.

In order to calculate the decay rates of sparticles, we pipe the output of the SOFTSUSY spectrum calculation through ISAWIG1.200. This is linked to ISAJET7.64 [85] in order to calculate the 2-body partial widths of the sparticles and Higgs'. The output from this procedure is fed into a specially modified version of the HERWIG program [86] that is able to calculate partial widths for the 2- and 4-body stau decays [87]. We shall now display the decay branching ratios for sparticles and Higgs'. We omit h^0 decays since these follow those of the standard model limit very closely.

The decays for benchmark point BC1 can be seen in Table IV. Here and in the following tables of benchmark points, for decays into the light quark flavors the results are summed over the flavors $q = u, s, d, c$. We see that, as designed, the $\tilde{\tau}_1$-LSP is completely dominated by 4-body decays. Each 4-body decay is accompanied by a tau. Thus good tau identification would help to identify this scenario. Furthermore, each 4-body decay includes a final-state neutrino, resulting in missing transverse momentum, $\not{p}_T$. This should however be reduced compared to a P_6 model, since the stau momentum is diluted in the 4-body decay. Also, the left-handed selectron and sneutrinos undergo significant $\not{P}_6$ decays. The heavier neutralinos have significant branching ratios into charginos as well as Z^0-bosons/Higgs and lighter neutralinos. The number of expected taus from a given SUSY pair production event is often 4 or more. We also see a difference in the decays of $\tilde{e}_R$ and $\tilde{\mu}_R$ due to the presence of the λ_{121} coupling. Furthermore, we see from the table that other $\not{P}_6$ couplings that are induced in the RGE running are not large enough to induce branching ratios greater than 0.005.

The decays for benchmark point BC2 can be seen in Table V. We see that, as designed, the $\tilde{\tau}_1$-LSP is completely dominated by 2-body decays into non-b jets. Unlike BC1, the LSP decay comes without a neutrino, meaning that SUSY events do not necessarily possess the classic missing transverse momentum $\not{p}_T$ signature. A comparison between Tables V and IV shows that many of the decays are identical as a result of the spectrum being approximately identical. The main differences are in the light sparticle decays: $\tilde{\tau}_1$, $\tilde{e}_{L,R}$, $\tilde{\mu}_{L,R}$, and $\tilde{\nu}_{e,\mu}$. The λ'_{311} coupling is too small to have a significant affect upon squark decays. However, in a collider the main difference will be the existence of detached vertices from the relatively long-lived $\tilde{\tau}_1$, which has a lifetime of $\tau_{\tilde{\tau}_1} = 1.1 \times 10^{-12}$ sec in its rest-frame. This corresponds to a rest-frame decay

TABLE IV. Sparticle and Higgs decays for BC1: $\lambda_{121}(M_{\rm GUT}) = 0.032$, $\tan\beta = 13$, $M_{1/2} = 400$ GeV, $M_0 = A_0 = 0$, $\mathrm{sgn}(\mu) = +1$. $\not{p}_6$ decays are shown in bold font. Only decays with branching ratios greater or equal 0.5% are shown. All decays are prompt. The spectrum is displayed in Fig. 9.

	Channel	BR	Channel	BR
$\tilde{\tau}_1$	$\mu^+\bar{\nu}_e e^-\tau^-$	**0.322**	$e^+\bar{\nu}_\mu e^-\tau^-$	**0.321**
	$\mu^-\nu_e e^+\tau^-$	**0.179**	$e^-\nu_\mu e^+\tau^-$	**0.178**
$\tilde{\chi}_1^0$	$\tilde{\tau}_1^+\tau^-$	0.498	$\tilde{\tau}_1^-\tau^+$	0.498
$\tilde{e}_R$	$e^-\nu_\mu$	**0.500**	$\mu^-\nu_e$	**0.500**
$\tilde{\mu}_R$	$\tilde{\tau}^+\mu^-\tau^-$	0.512	$\tilde{\tau}^-\mu^-\tau^+$	0.487
$\tilde{\tau}_2$	$\tilde{\chi}_1^0\tau^-$	0.630	$Z^0\tilde{\tau}_1^-$	0.176
	$h^0\tilde{\tau}_1^-$	0.194		
$\tilde{\nu}_e(\tilde{\nu}_\mu)$	$\tilde{\chi}_1^0\nu_e(\nu_\mu)$	0.924	$\mu^+(e^+)e^-$	**0.075**
$\tilde{\nu}_\tau$	$\tilde{\chi}_1^0\nu_\tau$	0.672	$W^+\tilde{\tau}_1$	0.328
$\tilde{e}_L^-(\tilde{\mu}_L^-)$	$\tilde{\chi}_1^0 e^-(\mu^-)$	0.919	$e^-\bar{\nu}_\mu(\bar{\nu}_e)$	**0.081**
$\tilde{d}_L(\tilde{s}_L)$	$\tilde{\chi}_1^- u(c)$	0.616	$\tilde{\chi}_2^0 d(s)$	0.313
	$\tilde{\chi}_2^- u(c)$	0.038	$\tilde{\chi}_1^0 d(s)$	0.018
	$\tilde{\chi}_4^0 d(s)$	0.014		
$\tilde{u}_L(\tilde{c}_L)$	$\tilde{\chi}_1^+ d(s)$	0.646	$\tilde{\chi}_2^0 u(c)$	0.318
	$\tilde{\chi}_2^+ d(s)$	0.015	$\tilde{\chi}_4^0 u(c)$	0.011
	$\tilde{\chi}_1^0 u(c)$	0.010		
$\tilde{d}_R(\tilde{s}_R)$	$\tilde{\chi}_1^0 d(s)$	0.994		
$\tilde{u}_R(\tilde{c}_R)$	$\tilde{\chi}_1^0 u(c)$	0.994		
$\tilde{b}_1$	$\tilde{\chi}_1^- t$	0.360	$\tilde{\chi}_2^- t$	0.252
	$\tilde{\chi}_2^0 b$	0.220	$W^-\tilde{t}_1$	0.120
	$\tilde{\chi}_1^0 b$	0.024	$\tilde{\chi}_3^0 b$	0.012
	$\tilde{\chi}_4^0 b$	0.011		
$\tilde{b}_2$	$\tilde{\chi}_2^- t$	0.408	$W^-\tilde{t}_1$	0.152
	$\tilde{\chi}_1^- t$	0.100	$\tilde{\chi}_1^0 b$	0.127
	$\tilde{\chi}_4^0 b$	0.086	$\tilde{\chi}_3^0 b$	0.067
	$\tilde{\chi}_2^0 b$	0.060		
$\tilde{t}_1$	$\tilde{\chi}_1^+ b$	0.440	$\tilde{\chi}_1^0 t$	0.237
	$\tilde{\chi}_2^+ b$	0.170	$\tilde{\chi}_2^0 t$	0.154
$\tilde{t}_2$	$\tilde{\chi}_4^0 t$	0.235	$\tilde{\chi}_1^+ b$	0.230
	$\tilde{\chi}_2^+ b$	0.150	$Z^0\tilde{t}_1$	0.123
	$\tilde{\chi}_3^0 t$	0.096	$\tilde{\chi}_2^0 t$	0.096
	$h^0 t$	0.057	$\tilde{\chi}_1^0 t$	0.023
H^0	$b\bar{b}$	0.854	$\tau^-\tau^+$	0.065
	$t\bar{t}$	0.046	$\tilde{\tau}_2^-\tilde{\tau}_1^+$	0.009
	$\tilde{\tau}_1^-\tilde{\tau}_2^+$	0.009	$\tilde{\chi}_1^0\tilde{\chi}_2^0$	0.007
A^0	$b\bar{b}$	0.826	$\tau^-\tau^+$	0.063
	$t\bar{t}$	0.061	$\tilde{\chi}_1^0\tilde{\chi}_2^0$	0.023
H^-	$\bar{t}b$	0.853	$\bar{\nu}_\tau\tau^-$	0.080
	$\tilde{\chi}_1^-\tilde{\chi}_1^0$	0.036	$\tilde{\tau}_1^-\bar{\tilde{\nu}}_\tau$	0.028

TABLE IV. (*Continued*)

	Channel	BR	Channel	BR
$\tilde{\chi}_2^0$	$\tilde{\nu}_\tau\bar{\nu}_\tau$	0.091	$\bar{\tilde{\nu}}_\tau\nu_\tau$	0.091
	$\tilde{\nu}_\mu\bar{\nu}_\mu$	0.085	$\bar{\tilde{\nu}}_\mu\nu_\mu$	0.085
	$\tilde{\nu}_e\bar{\nu}_e$	0.085	$\bar{\tilde{\nu}}_e\nu_e$	0.085
	$\tilde{\tau}_1^-\tau^+$	0.091	$\tilde{\tau}_1^+\tau^-$	0.091
	$\tilde{\mu}_L^-\mu^+$	0.045	$\tilde{\mu}_L^+\mu^-$	0.045
	$\tilde{e}_L^- e^+$	0.045	$\tilde{e}_L^+ e^-$	0.045
	$\tilde{\tau}_2^-\tau^+$	0.031	$\tilde{\tau}_2^+\tau^-$	0.031
	$\tilde{\chi}_1^0 h^0$	0.035		
$\tilde{\chi}_3^0$	$\tilde{\chi}_1^- W^+$	0.289	$\tilde{\chi}_1^+ W^-$	0.289
	$\tilde{\chi}_2^0 Z^0$	0.241	$\tilde{\chi}_1^0 Z^0$	0.102
	$\tilde{\chi}_1^0 h^0$	0.018	$\tilde{\tau}_1^-\tau^+$	0.010
	$\tilde{\tau}_1^+\tau^-$	0.010	$\tilde{\tau}_2^-\tau^+$	0.008
	$\tilde{\tau}_2^+\tau^-$	0.009	$\tilde{\chi}_2^0 h^0$	0.008
$\tilde{\chi}_4^0$	$\tilde{\chi}_1^- W^+$	0.265	$\tilde{\chi}_1^+ W^-$	0.265
	$\tilde{\chi}_2^0 h^0$	0.175	$\tilde{\chi}_1^0 h^0$	0.071
	$\tilde{\nu}_\tau\bar{\nu}_\tau$	0.018	$\bar{\tilde{\nu}}_\tau\nu_\tau$	0.018
	$\tilde{\nu}_\mu\bar{\nu}_\mu$	0.018	$\bar{\tilde{\nu}}_\mu\nu_\mu$	0.018
	$\tilde{\nu}_e\bar{\nu}_e$	0.018	$\bar{\tilde{\nu}}_e\nu_e$	0.018
	$\tilde{\tau}_2^-\tau^+$	0.017	$\tilde{\tau}_2^+\tau^-$	0.017
	$\tilde{\chi}_1^0 Z^0$	0.018	$\tilde{\chi}_2^0 Z^0$	0.014
	$\tilde{\mu}_L^-\mu^+$	0.008	$\tilde{\mu}_L^+\mu^-$	0.008
	$\tilde{e}_L^- e^+$	0.008	$\tilde{e}_L^+ e^-$	0.008
	$\tilde{\tau}_1^\mp\tau^\pm$	0.005		
$\tilde{\chi}_1^-$	$\tilde{\nu}_\tau\tau^-$	0.202	$\tilde{\nu}_\mu\mu^-$	0.186
	$\tilde{\nu}_e e^-$	0.186	$\tilde{\tau}_1\bar{\nu}_\tau$	0.167
	$\tilde{\mu}_L\bar{\nu}_\mu$	0.081	$\tilde{e}_L\bar{\nu}_e$	0.081
	$\tilde{\tau}_2\bar{\nu}_\tau$	0.055	$\tilde{\chi}_1^0 W^-$	0.040
$\tilde{\chi}_2^-$	$\tilde{\chi}_2^0 W^-$	0.283	$\tilde{\chi}_1^- Z^0$	0.253
	$\tilde{\chi}_1^- h^0$	0.198	$\tilde{\chi}_1^0 W^-$	0.081
	$\tilde{\tau}_2\bar{\nu}_\tau$	0.044	$\tilde{\mu}_L\bar{\nu}_\mu$	0.037
	$\tilde{e}_L\bar{\nu}_e$	0.037	$\bar{\tilde{\nu}}_\tau\tau^-$	0.028
	$\bar{\tilde{\nu}}_\mu\mu^-$	0.016	$\bar{\tilde{\nu}}_e e^-$	0.016
	$\tilde{\tau}_1\bar{\nu}_\tau$	0.006		
$\tilde{g}$	$\tilde{t}_1\bar{t}$	0.095	$\bar{\tilde{t}}_1 t$	0.095
	$\tilde{b}_1\bar{b}$	0.077	$\bar{\tilde{b}}_1 b$	0.077
	$\tilde{b}_2\bar{b}$	0.052	$\bar{\tilde{b}}_2 b$	0.052
	$\tilde{q}\,\bar{q}$	0.250	$\bar{\tilde{q}} q$	0.250

length of $c\tau_{\tilde{\tau}_1} \approx 0.3$ mm. However, when this is boosted into the lab frame (for example by a factor $\gamma = 30$), then the decay-length becomes about 1 cm. If these $\tilde{\tau}$-LSPs come from other sparticle decays, one can expect a coincidence of detached vertices with other particles originating from the interaction point in the detector. Of course the number of decays will fall approximately exponentially with radial distance, and so one may obtain decays at radial distances of μm-mm, possibly interfering with b-tagging. We leave any in-depth study of such effects to future work using the benchmarks.

The decays for benchmark point BC3 are shown in Table VI. Here the tau sneutrino is the LSP and it necessarily couples to the dominant $\not{p}_6$ operator. Therefore it will always decay via the 2-body mode to the purely

TABLE V. Sparticle and Higgs decays for BC2: $\lambda'_{311}(M_{\rm GUT}) = 3.5 \times 10^{-7}$, $\tan\beta = 13$, $M_{1/2} = 400$ GeV, $M_0 = A_0 = 0$. $\not{p}_6$ decays are shown in bold font. Only decays with branching ratios greater than 0.005 are shown. In the tenth row $\tilde{q}_R = \tilde{d}_R$, $\tilde{s}_R$, $\tilde{u}_R$, $\tilde{c}_R$. And the q in the decays is correspondingly $q = d$, s, u, c. All decays are prompt except for $\tilde{\tau}_1$, which has a lifetime of 1.1×10^{-12} secs. The spectrum is shown in Fig. 9.

	Channel	BR	Channel	BR
$\tilde{\tau}_1$	$\bar{u}d$	**1.000**		
$\tilde{\chi}_1^0$	$\tilde{\tau}_1^+\tau^-$	0.500	$\tilde{\tau}_1^-\tau^+$	0.500
$\tilde{e}_R(\tilde{\mu}_R)$	$\tilde{\tau}_1^+ e^-(\mu^-)\tau^-$	0.512	$\tilde{\tau}_1^- e^-(\mu^-)\tau^+$	0.488
$\tilde{\tau}_2$	$\tilde{\chi}_1^0\tau^-$	0.629	$Z^0\tilde{\tau}_1^-$	0.176
	$h^0\tilde{\tau}_1^-$	0.145		
$\tilde{\nu}_e(\tilde{\nu}_\mu)$	$\tilde{\chi}_1^0\nu_e(\nu_\mu)$	1.000		
$\tilde{\nu}_\tau$	$\tilde{\chi}_1^0\nu_\tau$	0.672	$W^+\tilde{\tau}_1$	0.328
$\tilde{e}_L^-(\tilde{\mu}_L^-)$	$\tilde{\chi}_1^0 e^-(\mu^-)$	1.000		
$\tilde{d}_L(\tilde{s}_L)$	$\tilde{\chi}_1^- u(c)$	0.616	$\tilde{\chi}_2^0 d(s)$	0.313
	$\tilde{\chi}_2^- u(c)$	0.038	$\tilde{\chi}_1^0 d(s)$	0.018
	$\tilde{\chi}_4^0 d(s)$	0.014		
$\tilde{u}_L(\tilde{c}_L)$	$\tilde{\chi}_1^+ d(s)$	0.646	$\tilde{\chi}_2^0 u(c)$	0.318
	$\tilde{\chi}_2^+ d(s)$	0.015	$\tilde{\chi}_4^0 u(c)$	0.011
	$\tilde{\chi}_1^0 u(c)$	0.010		
$\tilde{q}_R$	$\tilde{\chi}_1^0 q$	0.994	$\tilde{\chi}_4^0 q$	0.003
	$\tilde{\chi}_2^0 q$	0.002		
$\tilde{b}_1$	$\tilde{\chi}_1^- t$	0.355	$\tilde{\chi}_2^- t$	0.252
	$\tilde{\chi}_2^0 b$	0.220	$W^-\tilde{t}_1$	0.120
	$\tilde{\chi}_1^0 b$	0.024	$\tilde{\chi}_3^0 b$	0.012
	$\tilde{\chi}_4^0 b$	0.011		
$\tilde{b}_2$	$\tilde{\chi}_2^- t$	0.408	$W^-\tilde{t}_1$	0.152
	$\tilde{\chi}_1^- t$	0.100	$\tilde{\chi}_1^0 b$	0.127
	$\tilde{\chi}_4^0 b$	0.086	$\tilde{\chi}_3^0 b$	0.067
	$\tilde{\chi}_2^0 b$	0.060		
$\tilde{t}_1$	$\tilde{\chi}_1^+ b$	0.440	$\tilde{\chi}_1^0 t$	0.237
	$\tilde{\chi}_2^+ b$	0.169	$\tilde{\chi}_2^0 t$	0.154
$\tilde{t}_2$	$\tilde{\chi}_4^0 t$	0.235	$\tilde{\chi}_1^+ b$	0.220
	$\tilde{\chi}_2^+ b$	0.150	$Z^0\tilde{t}_1$	0.123
	$\tilde{\chi}_3^0 t$	0.096	$\tilde{\chi}_2^0 t$	0.096
	$h^0 t$	0.056	$\tilde{\chi}_1^0 t$	0.023
$\tilde{\chi}_2^0$	$\tilde{\nu}_\tau\bar{\nu}_\tau$	0.091	$\bar{\tilde{\nu}}_\tau\nu_\tau$	0.091
	$\tilde{\nu}_\mu\bar{\nu}_\mu$	0.085	$\bar{\tilde{\nu}}_\mu\nu_\mu$	0.085
	$\tilde{\nu}_e\bar{\nu}_e$	0.085	$\bar{\tilde{\nu}}_e\nu_e$	0.085
	$\tilde{\tau}_1^-\tau^+$	0.092	$\tilde{\tau}_1^+\tau^-$	0.092
	$\tilde{\mu}_L^-\mu^+$	0.044	$\tilde{\mu}_L^+\mu^-$	0.044
	$\tilde{e}_L^-e^+$	0.044	$\tilde{e}_L^+e^-$	0.044
	$\tilde{\tau}_2^-\tau^+$	0.031	$\tilde{\tau}_2^+\tau^-$	0.031
	$\tilde{\chi}_1^0 h^0$	0.035		
$\tilde{\chi}_3^0$	$\tilde{\chi}_1^- W^+$	0.289	$\tilde{\chi}_1^+ W^-$	0.289
	$\tilde{\chi}_2^0 Z^0$	0.241	$\tilde{\chi}_1^0 Z^0$	0.102
	$\tilde{\chi}_1^0 h^0$	0.018	$\tilde{\tau}_1^-\tau^+$	0.010
	$\tilde{\tau}_1^+\tau^-$	0.010	$\tilde{\tau}_2^-\tau^+$	0.008
	$\tilde{\tau}_2^+\tau^-$	0.008	$\tilde{\chi}_2^0 h^0$	0.009
$\tilde{\chi}_4^0$	$\tilde{\chi}_1^- W^+$	0.265	$\tilde{\chi}_1^+ W^-$	0.265
	$\tilde{\chi}_2^0 h^0$	0.175	$\tilde{\chi}_1^0 h^0$	0.072
	$\tilde{\nu}_\tau\bar{\nu}_\tau$	0.018	$\bar{\tilde{\nu}}_\tau\nu_\tau$	0.018
	$\tilde{\nu}_\mu\bar{\nu}_\mu$	0.018	$\bar{\tilde{\nu}}_\mu\nu_\mu$	0.018
	$\tilde{\nu}_e\bar{\nu}_e$	0.018	$\bar{\tilde{\nu}}_e\nu_e$	0.018
	$\tilde{\tau}_2^-\tau^+$	0.017	$\tilde{\tau}_2^+\tau^-$	0.017
	$\tilde{\chi}_1^0 Z^0$	0.018	$\tilde{\chi}_2^0 Z^0$	0.014
	$\tilde{\mu}_L^-\mu^+$	0.008	$\tilde{\mu}_L^+\mu^-$	0.008
	$\tilde{e}_L^-e^+$	0.008	$\tilde{e}_L^+e^-$	0.008
	$\tilde{\tau}_1^-\tau^+$	0.005	$\tilde{\tau}_1^+\tau^-$	0.005
$\tilde{\chi}_1^-$	$\tilde{\nu}_\tau\tau^-$	0.203	$\tilde{\nu}_\mu\mu^-$	0.186
	$\tilde{\nu}_e e^-$	0.186	$\tilde{\tau}_1\bar{\nu}_\tau$	0.168
	$\tilde{\mu}_L\bar{\nu}_\mu$	0.081	$\tilde{e}_L\bar{\nu}_e$	0.081
	$\tilde{\tau}_2\bar{\nu}_\tau$	0.060	$\tilde{\chi}_1^0 W^-$	0.040
$\tilde{\chi}_2^-$	$\tilde{\chi}_2^0 W^-$	0.283	$\tilde{\chi}_1^- Z^0$	0.253
	$\tilde{\chi}_1^- h^0$	0.198	$\tilde{\chi}_1^0 W^-$	0.082
	$\tilde{\tau}_2\bar{\nu}_\tau$	0.044	$\tilde{\mu}_L\bar{\nu}_\mu$	0.037
	$\tilde{e}_L\bar{\nu}_e$	0.037	$\bar{\tilde{\nu}}_\tau\tau^-$	0.028
	$\bar{\tilde{\nu}}_\mu\mu^-$	0.016	$\bar{\tilde{\nu}}_e e^-$	0.016
	$\tilde{\tau}_1\bar{\nu}_\tau$	0.006		
$\tilde{g}$	$\tilde{t}_1\bar{t}$	0.095	$\bar{\tilde{t}}_1 t$	0.095
	$\tilde{b}_1\bar{b}$	0.077	$\bar{\tilde{b}}_1 b$	0.077
	$\tilde{b}_2\bar{b}$	0.052	$\bar{\tilde{b}}_2 b$	0.052
	$\tilde{q}\,\bar{q}$	0.250	$\bar{\tilde{q}}q$	0.250
H^0	$b\bar{b}$	0.854	$\tau^-\tau^+$	0.065
	$t\bar{t}$	0.046	$\tilde{\chi}_1^0\tilde{\chi}_2^0$	0.007
	$\tilde{\tau}_2^-\tilde{\tau}_1^+$	0.009	$\tilde{\tau}_1^-\tilde{\tau}_2^+$	0.009
A^0	$b\bar{b}$	0.826	$\tau^-\tau^+$	0.063
	$t\bar{t}$	0.061	$\tilde{\chi}_1^0\tilde{\chi}_2^0$	0.023
H^-	$\bar{t}b$	0.853	$\bar{\nu}_\tau\tau^-$	0.080
	$\tilde{\chi}_1^-\tilde{\chi}_1^0$	0.036	$\tilde{\tau}_1^-\bar{\tilde{\nu}}_\tau$	0.028

hadronic final state $b\bar{d}$ ($\bar{b}d$). One of the daughter jets involves a bottom quark, providing for the possibility of using b-tagging in order to help identify SUSY events. The neutralino is the NLSP and the only decay mode open is the 2 body decay to $\tilde{\nu}_\tau\bar{\nu}_\tau$ ($\tilde{\nu}_\tau^*\nu_\tau$), which results in missing $p_{\rm T}$ in the final state. Both $\tilde{\chi}_1^\pm$ and $\tilde{\chi}_2^0$ have significant branching ratios to tau leptons/stau sleptons. Thus the cascade decays of left-handed squarks and indirectly thus also the gluinos should still lead to significant number of taus in the final state. We also see from the table that other $\not{P}_6$ couplings that are induced in the RGE running are not sufficiently large to induce branching ratios greater than 0.005.

We display the decays for benchmark point BC4 in Table VII. Here, the $\tilde{\tau}_1$-LSP decays exclusively into a τ and 3 non-b jets, since the decays via a virtual chargino are

TABLE VI. Sparticle and Higgs decays for BC3: $\lambda'_{331}(M_{\rm GUT}) = 0.122$, $\tan\beta = 10$, $M_{1/2} = 250$ GeV, $M_0 = 100$ GeV, $A_0 = -100$ GeV. $\not{P}_6$ decays are shown in bold font. Only decays with branching ratios greater than 0.005 are shown. All decays are prompt.

	Channel	BR	Channel	BR
$\tilde{\nu}_\tau$	$\bar{b}d$	**1.000**		
$\tilde{\chi}_1^0$	$\bar{\tilde{\nu}}_\tau\nu_\tau$	0.500	$\tilde{\nu}_\tau\bar{\nu}_\tau$	0.500
$\tilde{\tau}_1^-$	$\nu_\tau b\bar{d}\tau^-$	**0.372**	$\bar{\nu}_\tau\,\bar{b}\,d\tau^-$	**0.372**
	$\tilde{\chi}_1^0\tau^-$	0.256		
$\tilde{\tau}_2^-$	$\tilde{\chi}_1^0\tau^-$	1.000		
$\tilde{\nu}_e(\tilde{\nu}_\mu)$	$\tilde{\chi}_1^0\nu_e(\nu_\mu)$	0.852	$\tilde{\chi}_1^+e^-(\mu^-)$	0.107
	$\tilde{\chi}_2^0\nu_e(\nu_\mu)$	0.041		
$\tilde{e}_L^-(\tilde{\mu}_L^-)$	$\tilde{\chi}_1^0e^-(\mu^-)$	0.476	$\tilde{\chi}_1^-\bar{\nu}_e(\bar{\nu}_\mu)$	0.331
	$\tilde{\chi}_2^0e^-(\mu^-)$	0.192		
$\tilde{e}_R^-(\tilde{\mu}_R^-)$	$\tilde{\chi}_1^0e^-(\mu^-)$	1.000		
$\tilde{d}_L(\tilde{s}_L)$	$\tilde{\chi}_1^-u(c)$	0.604	$\tilde{\chi}_2^0d(s)$	0.307
	$\tilde{\chi}_2^-u(c)$	0.047	$\tilde{\chi}_1^0d(s)$	0.024
	$\tilde{\chi}_4^0d(s)$	0.017		
$\tilde{d}_R$	$\nu_\tau b$	**0.494**	τ^-t	**0.397**
	$\tilde{\chi}_1^0d$	0.108		
$\tilde{s}_R(\tilde{u}_R,\tilde{c}_R)$	$\tilde{\chi}_1^0s(u,c)$	0.985	$\tilde{\chi}_2^0s(u,c)$	0.010
$\tilde{u}_L(\tilde{c}_L)$	$\tilde{\chi}_1^+d(s)$	0.650	$\tilde{\chi}_2^0u(c)$	0.317
	$\tilde{\chi}_2^+d(s)$	0.015	$\tilde{\chi}_4^0u(c)$	0.012
	$\tilde{\chi}_1^0u(c)$	0.006		
$\tilde{b}_1$	$\tilde{\chi}_1^-t$	0.350	$\tilde{\chi}_2^0b$	0.275
	$\bar{\nu}_\tau d$	**0.219**	$W^-\tilde{t}_1$	0.106
	$\tilde{\chi}_1^0b$	0.032	$\tilde{\chi}_4^0b$	0.011
	$\tilde{\chi}_3^0b$	0.007		
$\tilde{b}_2$	$\tilde{\chi}_1^0b$	0.321	$W^-\tilde{t}_1$	0.217
	$\bar{\nu}_\tau d$	**0.125**	$\tilde{\chi}_4^0b$	0.108
	$\tilde{\chi}_3^0b$	0.093	$\tilde{\chi}_1^-t$	0.076
	$\tilde{\chi}_2^0b$	0.060		
$\tilde{t}_1$	$\tilde{\chi}_1^+b$	0.600	$\tilde{\chi}_1^0t$	0.157
	τ^+d	**0.124**	$\tilde{\chi}_2^0t$	0.108
	$\tilde{\chi}_2^+b$	0.010		
$\tilde{t}_2$	$\tilde{\chi}_2^+b$	0.191	$\tilde{\chi}_4^0t$	0.185
	$\tilde{\chi}_1^+b$	0.176	$Z^0\tilde{t}_1$	0.169
	τ^+d	**0.108**	$\tilde{\chi}_2^0t$	0.071
	$\tilde{\chi}_3^0t$	0.041	$h^0\tilde{t}_1$	0.033
	$\tilde{\chi}_1^0t$	0.027		
$\tilde{\chi}_2^0$	$\bar{\tilde{\nu}}_\tau\nu_\tau$	0.270	$\tilde{\nu}_\tau\bar{\nu}_\tau$	0.270
	$\tilde{\tau}_1^+\tau^-$	0.219	$\tilde{\tau}_1^-\tau^+$	0.219
	$\tilde{\tau}_2^+\tau^-$	0.009	$\tilde{\tau}_2^-\tau^+$	0.009
$\tilde{\chi}_3^0$	$\tilde{\chi}_1^-W^+$	0.295	$\tilde{\chi}_1^+W^-$	0.295
	$\tilde{\chi}_2^0Z^0$	0.212	$\tilde{\chi}_1^0Z^0$	0.109
	$\tilde{\chi}_1^0h^0$	0.020	$\tilde{\chi}_2^0h^0$	0.011
	$\tilde{\tau}_2^-\tau^+$	0.011	$\tilde{\tau}_2^+\tau^-$	0.011
	$\bar{\tilde{\tau}}_\tau\nu_\tau$	0.005	$\tilde{\nu}_\tau\bar{\nu}_\tau$	0.005
$\tilde{\chi}_4^0$	$\tilde{\chi}_1^-W^+$	0.252	$\tilde{\chi}_1^+W^-$	0.252
	$\tilde{\chi}_2^0h^0$	0.127	$\tilde{\chi}_1^0h^0$	0.062
	$\tilde{\nu}_\tau\bar{\nu}_\tau$	0.037	$\bar{\tilde{\nu}}_\tau\nu_\tau$	0.037
	$\tilde{\nu}_\mu\bar{\nu}_\mu$	0.024	$\bar{\tilde{\nu}}_\mu\nu_\mu$	0.024
	$\tilde{\nu}_e\bar{\nu}_e$	0.013	$\bar{\tilde{\nu}}_e\nu_e$	0.013
	$\tilde{\chi}_1^0Z^0$	0.020	$\tilde{\tau}_2^-\tau^+$	0.019
	$\tilde{\tau}_2^+\tau^-$	0.019	$\tilde{\chi}_2^0Z^0$	0.018
	$\tilde{\mu}_L^-\mu^+$	0.009	$\tilde{\mu}_L^+\mu^-$	0.009
	$\tilde{e}_L^-e^+$	0.009	$\tilde{e}_L^+e^-$	0.009
$\tilde{\chi}_1^-$	$\tilde{\nu}_\tau\tau^-$	0.632	$\tilde{\tau}_1^-\nu_\tau$	0.354
	$\tilde{\tau}_2^-\nu_\tau$	0.013		
$\tilde{\chi}_2^-$	$\tilde{\chi}_2^0W^-$	0.284	$\tilde{\chi}_1^-Z^0$	0.233
	$\tilde{\chi}_1^-h^0$	0.161	$\tilde{\chi}_1^0W^-$	0.062
	$\tilde{\mu}_L^-\bar{\nu}_\mu$	0.050	$\tilde{e}_L^-\bar{\nu}_e$	0.050
	$\tilde{\tau}_2^-\bar{\nu}_\tau$	0.048	$\bar{\tilde{\nu}}_\tau\tau^-$	0.039
	$\tilde{\tau}_1^-\bar{\nu}_\tau$	0.035	$\bar{\tilde{\nu}}_\mu\mu^-$	0.019
	$\bar{\tilde{\nu}}_e e^-$	0.019		
$\tilde{g}$	$\tilde{b}_1\bar{b}$	0.114	$\bar{\tilde{b}}_1 b$	0.114
	$\tilde{t}_1\bar{t}$	0.052	$\bar{\tilde{t}}_1 t$	0.052
	$\tilde{b}_2\bar{b}$	0.049	$\bar{\tilde{b}}_2 b$	0.049
	$\tilde{q}\,\bar{q}$	0.284	$\bar{\tilde{q}}q$	0.284
H^0	$b\bar{b}$	0.787	$\tau^-\tau^+$	0.057
	$t\bar{t}$	0.038	$\tilde{\chi}_1^0\tilde{\chi}_2^0$	0.035
	$\tilde{\chi}_1^+\tilde{\chi}_1^-$	0.026	$\tilde{\tau}_1^-\tilde{\tau}_1^+$	0.017
	$\tilde{\chi}_1^0\tilde{\chi}_1^0$	0.012	$\tilde{\chi}_2^0\tilde{\chi}_2^0$	0.010
	$\tilde{\tau}_2^-\tilde{\tau}_2^+$	0.006		
A^0	$b\bar{b}$	0.661	$t\bar{t}$	0.099
	$\tilde{\chi}_1^0\tilde{\chi}_2^0$	0.067	$\tilde{\chi}_2^0\tilde{\chi}_2^0$	0.058
	$\tau^-\tau^+$	0.048	$\tilde{\chi}_1^+\tilde{\chi}_1^-$	0.027
	$\tilde{\chi}_1^0\tilde{\chi}_1^0$	0.015	$\tilde{\tau}_1^-\tilde{\tau}_1^+$	0.010
	$\tilde{\tau}_1^-\tilde{\tau}_2^+$	0.007		
H^-	$\bar{t}b$	0.753	$\tilde{\chi}_1^-\tilde{\chi}_1^0$	0.130
	$\bar{\nu}_\tau\tau^-$	0.073	$\tilde{\tau}_1^-\bar{\tilde{\nu}}_\tau$	0.021
	$\tilde{\tau}_2^-\bar{\tilde{\nu}}_\tau$	0.015		

strongly suppressed, since the tau and the daughter quarks are dominantly $SU(2)$ singlets. Thus, this point will provide very little signal $\not{p}_T$. The first two generations of right-handed squarks undergo dominant $\not{p}_6$ decays into two jets, altering many LHC signatures. Aside from these, the decays are rather similar to those of BC3, as a comparison with Table VI shows, although some quantitative differences are present in every channel. The large number of jets in final states from this model could make analysis of SUSY events difficult: combinatoric backgrounds are likely in event reconstruction. Examining specific decay

TABLE VII. Sparticle and Higgs decays for BC4: $\lambda''_{212}(M_{\rm GUT}) = 0.5$, $\tan\beta = 30$, $M_{1/2} = 600$ GeV, $M_0 = A_0 = 0$. $\not{p}_6$ decays are shown in bold font. Only decays with branching ratios greater than 0.005 are shown. All decays are prompt.

	Channel	BR	Channel	BR
$\tilde{\tau}_1$	$cds\tau^-$	**0.794**	$\bar{c}\,\bar{d}\,\bar{s}\,\tau^-$	**0.206**
$\tilde{\chi}_1^0$	$\tilde{\tau}_1^+\tau^-$	0.466	$\tilde{\tau}_1^-\tau^+$	0.466
	$\tilde{\mu}_R^-\mu^+$	0.017	$\tilde{\mu}_R^+\mu^-$	0.017
	$\tilde{e}_R^-e^+$	0.017	$\tilde{e}_R^+e^-$	0.017
$\tilde{\tau}_2$	$Z^0\tilde{\tau}_1^-$	0.476	$h^0\tilde{\tau}_1^-$	0.377
	$\tilde{\chi}_1^0\tau^-$	0.148		
$\tilde{\nu}_e(\tilde{\nu}_\mu)$	$\tilde{\chi}_1^0\nu_e(\nu_\mu)$	1.000		
$\tilde{\nu}_\tau$	$W^+\tilde{\tau}_1$	0.885	$\tilde{\chi}_1^0\nu_\tau$	0.115
$\tilde{e}_L^-(\tilde{\mu}_L^-)$	$\tilde{\chi}_1^0e^-(\mu^-)$	1.000		
$\tilde{e}_R(\tilde{\mu}_R)$	$\tilde{\tau}_1^+e^-(\mu^-)\tau^-$	0.584	$\tilde{\tau}_1^-e^-(\mu^-)\tau^+$	0.416
$\tilde{d}_L(\tilde{s}_L)$	$\tilde{\chi}_1^-u(c)$	0.629	$\tilde{\chi}_2^0d(s)$	0.318
	$\tilde{\chi}_2^-u(c)$	0.026	$\tilde{\chi}_1^0d(s)$	0.016
	$\tilde{\chi}_4^0d(s)$	0.010		
$\tilde{d}_R(\tilde{s}_R)$	$\bar{c}\,\bar{s}(\bar{d})$	**0.988**	$\tilde{\chi}_1^0d(s)$	0.012
$\tilde{u}_L(\tilde{c}_L)$	$\tilde{\chi}_1^+d(s)$	0.648	$\tilde{\chi}_2^0u(c)$	0.320
	$\tilde{\chi}_1^0u(c)$	0.013	$\tilde{\chi}_2^+d(s)$	0.011
	$\tilde{\chi}_4^0u(c)$	0.008		
$\tilde{u}_R$	$\tilde{\chi}_1^0u$	0.997		
$\tilde{c}_R$	$\bar{s}\,\bar{d}$	**0.953**	$\tilde{\chi}_1^0c$	0.047
$\tilde{b}_1$	$\tilde{\chi}_1^-t$	0.367	$\tilde{\chi}_2^0b$	0.210
	$\tilde{\chi}_2^-t$	0.186	$W^-\tilde{t}_1$	0.077
	$\tilde{\chi}_3^0b$	0.070	$\tilde{\chi}_4^0b$	0.049
	$\tilde{\chi}_1^0b$	0.040		
$\tilde{b}_2$	$\tilde{\chi}_2^-t$	0.443	$W^-\tilde{t}_1$	0.133
	$\tilde{\chi}_4^0b$	0.125	$\tilde{\chi}_3^0b$	0.109
	$\tilde{\chi}_1^-t$	0.103	$\tilde{\chi}_2^0b$	0.061
	$\tilde{\chi}_1^0b$	0.026		
$\tilde{t}_1$	$\tilde{\chi}_1^+b$	0.243	$\tilde{\chi}_2^+b$	0.242
	$\tilde{\chi}_1^0t$	0.210	$\tilde{\chi}_3^0t$	0.170
	$\tilde{\chi}_2^0t$	0.100	$\tilde{\chi}_4^0t$	0.035
$\tilde{t}_2$	$\tilde{\chi}_1^+b$	0.239	$\tilde{\chi}_4^0t$	0.200
	$\tilde{\chi}_2^+b$	0.174	$\tilde{\chi}_3^0t$	0.109
	$\tilde{\chi}_2^0t$	0.105	$Z^0\tilde{t}_1$	0.091
	$h^0\tilde{t}_1$	0.061	$\tilde{\chi}_1^0t$	0.019
$\tilde{\chi}_2^0$	$\tilde{\tau}_1^+\tau^-$	0.127	$\tilde{\tau}_1^-\tau^+$	0.127
	$\tilde{\nu}_\tau\bar{\nu}_\tau$	0.086	$\bar{\tilde{\nu}}_\tau\nu_\tau$	0.086
	$\tilde{\nu}_\mu\bar{\nu}_\mu$	0.065	$\bar{\tilde{\nu}}_\mu\nu_\mu$	0.065
	$\tilde{\nu}_e\bar{\nu}_e$	0.064	$\bar{\tilde{\nu}}_e\nu_e$	0.064
	$\tilde{\mu}_L^-\mu^+$	0.054	$\tilde{\mu}_L^+\mu^-$	0.054
	$\tilde{e}_L^-e^+$	0.054	$\tilde{e}_L^+e^-$	0.054
	$\tilde{\tau}_2^-\tau^+$	0.041	$\tilde{\tau}_2^+\tau^-$	0.041
	$\tilde{\chi}_1^0h^0$	0.014		

TABLE VII. (*Continued*)

	Channel	BR	Channel	BR
$\tilde{\chi}_3^0$	$\tilde{\chi}_1^-W^+$	0.245	$\tilde{\chi}_1^+W^-$	0.245
	$\tilde{\chi}_2^0Z^0$	0.219	$\tilde{\chi}_1^0Z^0$	0.084
	$\tilde{\tau}_1^-\tau^+$	0.055	$\tilde{\tau}_1^+\tau^-$	0.055
	$\tilde{\tau}_2^-\tau^+$	0.033	$\tilde{\tau}_2^+\tau^-$	0.033
	$\tilde{\chi}_1^0h^0$	0.017	$\tilde{\chi}_2^0h^0$	0.008
$\tilde{\chi}_4^0$	$\tilde{\chi}_1^-W^+$	0.240	$\tilde{\chi}_1^+W^-$	0.240
	$\tilde{\chi}_2^0h^0$	0.186	$\tilde{\chi}_1^0h^0$	0.070
	$\tilde{\tau}_2^-\tau^+$	0.040	$\tilde{\tau}_2^+\tau^-$	0.040
	$\tilde{\tau}_1^-\tau^+$	0.037	$\tilde{\tau}_1^+\tau^-$	0.037
	$\tilde{\chi}_1^0Z^0$	0.017	$\tilde{\chi}_2^0Z^0$	0.011
	$\tilde{\nu}_\tau\bar{\nu}_\tau$	0.010	$\bar{\tilde{\nu}}_\tau\nu_\tau$	0.010
	$\tilde{\nu}_\mu\bar{\nu}_\mu$	0.010	$\bar{\tilde{\nu}}_\mu\nu_\mu$	0.010
	$\tilde{\nu}_e\bar{\nu}_e$	0.010	$\bar{\tilde{\nu}}_e\nu_e$	0.010
	$\tilde{\mu}_L^-\mu^+$	0.005	$\tilde{\mu}_L^+\mu^-$	0.005
	$\tilde{e}_L^-e^+$	0.005	$\tilde{e}_L^+e^-$	0.005
$\tilde{\chi}_1^-$	$\tilde{\tau}_1\bar{\nu}_\tau$	0.246	$\tilde{\nu}_\tau\tau^-$	0.185
	$\tilde{\nu}_\mu\mu^-$	0.136	$\tilde{\nu}_e e^-$	0.136
	$\tilde{\mu}_L\bar{\nu}_\mu$	0.103	$\tilde{e}_L\bar{\nu}_e$	0.103
	$\tilde{\tau}_2\bar{\nu}_\tau$	0.076	$\tilde{\chi}_1^0W^-$	0.016
$\tilde{\chi}_2^-$	$\tilde{\chi}_2^0W^-$	0.247	$\tilde{\chi}_1^-Z^0$	0.232
	$\tilde{\chi}_1^-h^0$	0.200	$\tilde{\chi}_1^0W^-$	0.085
	$\bar{\tilde{\nu}}_\tau\tau^-$	0.070	$\tilde{\tau}_1\bar{\nu}_\tau$	0.065
	$\tilde{\tau}_2\bar{\nu}_\tau$	0.041	$\tilde{\mu}_L\bar{\nu}_\mu$	0.020
	$\tilde{e}_L\bar{\nu}_e$	0.020	$\bar{\tilde{\nu}}_\mu\mu^-$	0.009
	$\bar{\tilde{\nu}}_e e^-$	0.009		
$\tilde{g}$	$\tilde{s}_R\bar{s}$	0.111	$\bar{\tilde{s}}_R s$	0.111
	$\tilde{d}_R\bar{d}$	0.111	$\bar{\tilde{d}}_R d$	0.111
	$\tilde{c}_R\bar{c}$	0.107	$\bar{\tilde{c}}_R c$	0.107
	$\tilde{t}_1\bar{t}$	0.049	$\bar{\tilde{t}}_1 t$	0.049
	$\tilde{b}_1\bar{b}$	0.035	$\bar{\tilde{b}}_1 b$	0.035
	$\tilde{b}_2\bar{b}$	0.025	$\bar{\tilde{b}}_2 b$	0.025
	$\tilde{q}\,\bar{q}$	0.062	$\bar{\tilde{q}}q$	0.062
H^0	$b\bar{b}$	0.776	$\tau^-\tau^+$	0.061
	$\tilde{\tau}_2^-\tilde{\tau}_1^+$	0.058	$\tilde{\tau}_1^-\tilde{\tau}_2^+$	0.058
	$\tilde{\tau}_1^-\tilde{\tau}_1^+$	0.042		
A^0	$b\bar{b}$	0.776	$\tau^-\tau^+$	0.061
	$\tilde{\tau}_2^-\tilde{\tau}_1^+$	0.058	$\tilde{\tau}_1^-\tilde{\tau}_2^+$	0.058
	$\tilde{\tau}_1^-\tilde{\tau}_1^+$	0.042		
H^-	$\bar{t}b$	0.733	$\tilde{\tau}_1^-\bar{\tilde{\nu}}_\tau$	0.193
	$\bar{\nu}_\tau\tau^-$	0.071		

chains involving leptons can help reduce these [88]. The combinatoric backgrounds problem will become worse for high luminosity running, where pile-up will increase the number of jets in each event. However, resonant squark production ought to be possible, providing an additional empirical handle on the model.

VII. CONCLUSIONS

We have investigated the spectrum of the $\not{R}_6$-MSSM embedded in supergravity, including indirect constraints on parameter space. We have found different regions of parameter space with a neutralino, a stau and also a tau sneutrino LSP. Taking these into account, we have presented the first set of benchmarks in $\not{R}_6$ mSUGRA. All of the points are within current search limits and are consistent with measurements of precision observables. We have picked different SUSY breaking scenarios: light and heavy. The heavier benchmarks are more difficult to detect at the LHC and so should be used to see how much is possible to achieve through data analyses in this difficult scenario. The light benchmarks are designed to enable high statistics analyses in order to determine what is possible to divine from LHC data in the optimistic case.

We have picked the flavor of the $\not{R}_6$ couplings in order to show-case various features relevant for the experiments. In the first benchmark, four-body decays of the LSP are expected including neutrinos, leading to complicated final states and $\not{p}_T$. The second benchmark has vertices detached from the interaction point, where LSPs decay into non-bottom jets. Coincidence with SM particles from higher up the cascades are expected from the interaction region. In the third, 2-body decays of a tau sneutrino LSP into jets (one of them a bottom jet) are expected. The fourth benchmark has LSPs promptly decaying into 3 jets and a tau. It also has a large $\not{R}_6$ coupling capable of producing significant single-squarks at hadron colliders such as the LHC. In order to enable analysis of the proposed benchmark points, we have provided HERWIG files on the web at URL address http://hepforge.cedar.ac.uk/~allanach/rpv/, where they are available for public download.

ACKNOWLEDGMENTS

M. B. and H. D. thank DAMTP, Cambridge, for warm hospitality offered while part of this work was performed as well as the SUSY working group at the Cavendish Laboratory, Cambridge, for discussions. H. D. also thanks the Aspen Center for Physics for hospitality while part of this work was performed and the participants of the LHC workshop for stimulating discussions on this work. We thank Sebastian Grab for computing some of the 4-body stau-LSP decays. We thank the Theoretical Condensed Matter Group, Bonn, for readily sharing computation resources, and Markus Schumacher for useful discussions on Higgs physics. This work was partially supported by PPARC.

APPENDIX A: $\not{R}_6$ CONTRIBUTION TO $\mathbf{Br}(B_{qk} \to e_m^+ e_l^-)$

Here, we generalize the calculation of Ref. [69] to include nondegenerate sparticle masses as well as squark mixing. The diagrams of interest consist of 2 s-channel diagrams mediated by sneutrinos, and a t-channel diagram mediated by left-handed up-type squarks. Using the convention of Ref. [53], we write the squark mixing as

$$\tilde{u}_{Lj} = c_j \tilde{u}_{1j} - s_j \tilde{u}_{2j}, \tag{A1}$$

where the $c_j \equiv \cos\theta_j^{\tilde{u}}$, $s_j \equiv \sin\theta_j^{\tilde{u}}$, $j = 1, 2, 3$ is a generation index and the states on the right hand side are mass eigenstates. For convenience, we define the following quantities:

$$A_{lm}^j = \sum_{i=1}^{3} \frac{\lambda_{ilm}^* \lambda'_{ij3}}{m^2_{\tilde{\nu}_i}}, \tag{A2}$$

$$B_{lm}^j = \sum_{i=1}^{3} \frac{\lambda_{iml}^* \lambda'_{i3j}}{m^2_{\tilde{\nu}_i}}, \tag{A3}$$

$$C_{lm}^j = \frac{1}{2} \sum_{i=1}^{3} \lambda'^*_{lij} \lambda'_{mi3} \left[\frac{c_i^2}{m^2_{\tilde{u}_{1i}}} + \frac{s_i^2}{m^2_{\tilde{u}_{2i}}} \right], \tag{A4}$$

$$\kappa_k = \frac{m_{e_k}}{M_{B_{q_j}}}. \tag{A5}$$

The final expression for the partial width of the decay $B_{q_j} \to e_m^+ e_l^-$ reads:

$$\Gamma = \frac{f_{B_{q_j}}^2 M_{B_{q_j}}^3}{64\pi} \sqrt{1 - 2(\kappa_m^2 + \kappa_l^2) + (\kappa_m^2 - \kappa_l^2)^2} \{ [(|A_{lm}^j|^2 + |B_{lm}^j|^2)(1 - \kappa_l^2 - \kappa_m^2) + 4\,\mathrm{Re}(A_{lm}^j B_{lm}^{j*})\kappa_l \kappa_m]$$
$$+ |C_{lm}^j|^2 [(\kappa_l^2 + \kappa_m^2) - (\kappa_l^2 - \kappa_m^2)^2] + 2\,\mathrm{Re}(A_{ml}^j C_{ml}^{j*})\kappa_m (1 + \kappa_l^2 - \kappa_m^2) + 2\,\mathrm{Re}(B_{ml}^j C_{ml}^{j*})\kappa_l (1 + \kappa_m^2 - \kappa_l^2) \}, \tag{A6}$$

where $f_{B_{q_j}}$, $M_{B_{q_j}}$ are the decay constant and mass of the B_{q_j} meson, respectively.

[1] E. Gildener, Phys. Rev. D **14**, 1667 (1976); M. Veltman, Acta Phys. Pol. B **12**, 437 (1981); N. Sakai, Z. Phys. C **11**, 153 (1981); E. Witten, Nucl. Phys. **B188**, 513 (1981).

[2] S. L. Glashow, Nucl. Phys. **22**, 579 (1961); S. Weinberg, Phys. Rev. Lett. **19**, 1264 (1967).

[3] J. Wess and B. Zumino, Nucl. Phys. **B70**, 39 (1974); For reviews of the SSM see Refs. [22,89–91].

[4] See, for example, the discussion in M. Drees, hep-ph/9611409.

[5] W. Armstrong *et al.* (ATLAS Collaboration), Technical Proposal Report No. CERN-LHCC-94-43 1994; CMS Collaboration, Technical Proposal, Report No. CERN-LHCC-96-45 1996.

[6] N. Sakai and T. Yanagida, Nucl. Phys. **B197**, 533 (1982); S. Weinberg, Phys. Rev. D **26**, 287 (1982).

[7] H. K. Dreiner, hep-ph/9707435.

[8] J. L. Goity and M. Sher, Phys. Lett. B **346**, 69 (1995); **385**, 500 (1996); A. Y. Smirnov and F. Vissani, Phys. Lett. B **380**, 317 (1996); Nucl. Phys. **B460(E)**, 37 (1996).

[9] G. Farrar and P. Fayet, Phys. Lett. B **76**, 575 (1978).

[10] H. K. Dreiner, C. Luhn, and M. Thormeier, Phys. Rev. D **73**, 075007 (2006).

[11] L. Ibanez and G. Ross, Phys. Lett. B **260**, 291 (1991).

[12] L. Ibanez and C. Lopez, Phys. Lett. B **126**, 54 (1983).

[13] L. Alvarez-Gaume, J. Polchinski, and M. B. Wise, Nucl. Phys. **B221**, 495 (1983).

[14] L. Ibanez and C. Lopez, Nucl. Phys. **B233**, 511 (1984); L. E. Ibanez, C. Lopez, and C. Munoz, Nucl. Phys. **B256**, 218 (1985).

[15] I. Hinchliffe *et al.*, Phys. Rev. D **55**, 5520 (1997); A. Bartl *et al.*, eConf C960625 1996 SUP112.

[16] M. Battaglia *et al.*, Eur. Phys. J. C **22**, 535 (2001); M. Carena *et al.*, Eur. Phys. J. C **26**, 601 (2003); G. L. Kane *et al.*, Phys. Rev. D **67**, 045008 (2003); B. C. Allanach, F. Quevedo, and K. Suruliz, J. High Energy Phys. 04 (2006) 040.

[17] B. C. Allanach *et al.*, in Proceedings of the Summer Study on the Future of Particle Physics, Snowmass, 2001; N. Graf, Eur. Phys. J. C **25**, 113 (2002).

[18] J. R. Ellis *et al.* Eur. Phys. J. C **24**, 311 (2002); M. Battaglia *et al.*, Eur. Phys. J. C **33**, 273 (2004).

[19] G. Azuelos *et al.*, hep-ph/0204031.

[20] B. C. Allanach, S. Kraml, and W. Porod, J. High Energy Phys. 03 (2003) 016.

[21] D. Z. Freedman, P. van Nieuwenhuizen, and S. Ferrara, Phys. Rev. D **13**, 3214 (1976); S. Deser and B. Zumino, Phys. Lett. B **62**, 335 (1976).

[22] H. P. Nilles, Phys. Rep. **110**, 1 (1984).

[23] J. R. Ellis, A. B. Lahanas, D. V. Nanopoulos, and K. Tamvakis, Phys. Lett. B **134**, 429 (1984).

[24] G. F. Giudice and R. Rattazzi, Phys. Rep. **322**, 419 (1999).

[25] L. Randall and R. Sundrum, Nucl. Phys. **B557**, 79 (1999); B. C. Allanach and A. Dedes, J. High Energy Phys. 06 (2000) 017; F. De Campos *et al.*, Nucl. Phys. **B623**, 47 (2002).

[26] H. E. Haber, Nucl. Phys. B, Proc. Suppl. **62**, 469 (1998).

[27] U. Amaldi, W. de Boer, and H. Furstenau, Phys. Lett. B **260**, 447 (1991); J. R. Ellis, S. Kelley, and D. V. Nanopoulos, Nucl. Phys. **B373**, 55 (1992); P. Langacker and N. Polonsky, Phys. Rev. D **47**, 4028 (1993); A. Dedes, A. B. Lahanas, and K. Tamvakis, Phys. Rev. D **53**, 3793 (1996).

[28] A. H. Chamseddine, R. Arnowitt, and P. Nath, Phys. Rev. Lett. **49**, 970 (1982); L. Alvarez-Gaume, M. Claudson, and M. Wise, Nucl. Phys. **B207**, 96 (1982); L. Ibanez, Phys. Lett. B **118**, 73 (1982); S. Soni and H. Weldon, Phys. Lett. B **126**, 215 (1983); N. Ohta, Prog. Theor. Phys. **70**, 542 (1983); L. Hall, J. Lykken, and S. Weinberg, Phys. Rev. D **27**, 2359 (1983).

[29] L. Ibanez and G. Ross, Phys. Lett. B **110**, 215 (1982).

[30] The Snowmass points and slopes also include one point with nonuniversal gaugino masses, i.e. which violates the premise given in Eq. (8). There are also points for the case of gauge or gaugino mediated supersymmetry breaking as well as anomaly mediated supersymmetry breaking.

[31] H. P. Nilles, M. Srednicki, and D. Wyler, Phys. Lett. B **120**, 346 (1983).

[32] J. Ellis *et al.*, Nucl. Phys. **B238**, 453 (1984).

[33] T. Hebbeker, Phys. Lett. B **470**, 259 (1999).

[34] R. Barate *et al.* (LEP Working Group for Higgs boson searches), Phys. Lett. B **565**, 61 (2003).

[35] E. Eichten, I. Hinchliffe, K. D. Lane, and C. Quigg, Rev. Mod. Phys. **56**, 579 (1984); **58**, 1065(E) (1986).

[36] J. R. Ellis *et al.*, Phys. Lett. B **134**, 429 (1984).

[37] B. C. Allanach, A. Dedes, and H. K. Dreiner, Phys. Rev. D **69**, 115002 (2004).

[38] R. Hempfling, Nucl. Phys. **B478**, 3 (1996); M. Hirsch *et al.*, Nucl. Phys. **B524**, 23 (1998); Phys. Rev. D **62**, 113008 (2000); **65**, 119901 (2002); hep-ph/0606082.

[39] B. de Carlos and P. L. White, Phys. Rev. D **54**, 3427 (1996); **55**, 4222 (1997).

[40] B. C. Allanach, A. Dedes, and H. K. Dreiner, Phys. Rev. D **60**, 056002 (1999).

[41] T. Besmer and A. Steffen, Phys. Rev. D **63**, 055007 (2001).

[42] I. Jack, D. R. T. Jones, and A. F. Kord, Phys. Lett. B **588**, 127 (2004).

[43] I. Jack, D. R. T. Jones, and A. F. Kord, Phys. Lett. B **632**, 703 (2006).

[44] L. J. Hall and M. Suzuki, Nucl. Phys. **B231**, 1984 (419).

[45] H. K. Dreiner and M. Thormeier, Phys. Rev. D **69**, 053002 (2004).

[46] E. Nardi, Phys. Rev. D **55**, 5772 (1997).

[47] A. Dedes, S. Rimmer, J. Rosiek, and M. Schmidt-Sommerfeld, Phys. Lett. B **627**, 161 (2005); A. Dedes, S. Rimmer, and J. Rosiek, hep-ph/0603225; A. Abada and M. Losada, Phys. Lett. B **492**, 310 (2000).

[48] For single resonant production at e^+e^--colliders see J. Erler, J. L. Feng, and N. Polonsky, Phys. Rev. Lett. **78**, 3063 (1997); and at HERA J. Butterworth and H. K. Dreiner, Nucl. Phys. B **397**, 3 (1993); For nonresonant production, see B. C. Allanach *et al.*, Phys. Lett. B **420**, 307 (1998).

[49] See for example: S. Dimopoulos *et al.*, Phys. Rev. D **41**, 2099 (1990); H. Dreiner, P. Richardson, and M. Seymour, Phys. Rev. D **63**, 055008 (2001), and references therein.

[50] H. Dreiner and G. G. Ross, Nucl. Phys. **B365**, 597 (1991).

[51] V. Barger, G. F. Giudice, and T. Han, Phys. Rev. D **40**, 2987 (1989); G. Bhattacharyya, Nucl. Phys. Proc. Suppl. A **52**, 83 (1997).

[52] B. C. Allanach, A. Dedes, and H. K. Dreiner, Phys. Rev. D **60**, 075014 (1999).
[53] B. C. Allanach, Comput. Phys. Commun. **143**, 305 (2002).
[54] K. Agashe and M. Graesser, Phys. Rev. D **54**, 4445 (1996).
[55] G. Belanger, F. Boudjema, A. Pukhov, and A. Semenov, Comput. Phys. Commun. **149**, 103 (2002); G. Belanger, F. Boudjema, A. Pukhov, and A. Semenov, hep-ph/0405253.
[56] S. Eidelman *et al.* (Particle Data Group), Phys. Lett. B **592**, 1 (2004).
[57] G. W. Bennett *et al.* (Muon $g-2$ Collaboration), Phys. Rev. Lett. **92**, 161802 (2004); Phys. Rev. D **73**, 072003 (2006).
[58] M. Davier, S. Eidelman, A. Hocker, and Z. Zhang, Eur. Phys. J. C **31**, 503 (2003).
[59] A. Höcker and W. Marciano in the Review of Particle Physics, 2006; W.-M. Yao *et al.*, J. Phys. G **33**, 1 (2006).
[60] J. E. Kim, Phys. Lett. B **520**, 298 (2001).
[61] Heavy Flavor Averaging Group (HFAG), hep-ex/0603003; http://www.slac.stanford.edu/xorg/hfag.
[62] P. Gambino and M. Misiak, Nucl. Phys. **B611**, 338 (2001); A. J. Buras *et al.*, Nucl. Phys. **B631**, 219 (2002).
[63] B. C. Allanach, A. Brignole, and L. E. Ibanez, J. High Energy Phys. 05 (2005) 030.
[64] The most recent CDF number is given at: http://www-cdf.fnal.gov/physics/new/bottom/060316.blessed-bsmumu3/.
[65] G. Buchalla and A. J. Buras, Nucl. Phys. **B400**, 225 (1993); M. Blanke, A. J. Buras, D. Guadagnoli, and C. Tarantino, hep-ph/0604057.
[66] S. R. Choudhury and N. Gaur, Phys. Lett. B **451**, 86 (1999).
[67] C. Bobeth, T. Ewerth, F. Kruger, and J. Urban, Phys. Rev. D **64**, 074014 (2001).
[68] A. Dedes, H. K. Dreiner, and U. Nierste, Phys. Rev. Lett. **87**, 251804 (2001).
[69] J. H. Jang, J. K. Kim, and J. S. Lee, Phys. Rev. D **55**, 7296 (1997).
[70] The maximal value $\lambda'_{331} = 0.15$ leads to a sneutrino mass which has been excluded by LEP.
[71] A. G. Akeroyd *et al.*, Nucl. Phys. **B529**, 3 (1998); A. De Gouvea, A. Friedland, and H. Murayama, Phys. Rev. D **59**, 095008 (1999); A. Bartl, M. Hirsch, T. Kernreiter, W. Porod, and J. W. F. Valle, J. High Energy Phys. 11 (2003) 005.
[72] At the LHC we also expect resonant slepton (squark) production for λ', $\lambda'' > 10^{-3}$, cf. Ref. [48].This requires a separate analysis. See also H. Dreiner, S. Grab, M. Krämer, and M. Trenkel, Aachen Report No. PITHA-06-10, Bonn Report No. BONN-TH-2006-06, as well as the Diplom theses of S. Grab (Bonn) and M. Trenkel (Aachen).
[73] We thank Sebastian Grab for sharing some of his computations.
[74] W. Buchmüller, K. Hamaguchi, M. Ratz, and T. Yanagida, Phys. Lett. B **588**, 90 (2004); J. L. Feng and B. T. Smith, Phys. Rev. D **71**, 015004(E) (2005); **71**, 015004 (2005); A. Brandenburg *et al.*, Phys. Lett. B **617**, 99 (2005). F. D. Steffen, J. Cosmol. Astropart. Phys. 09 (2006) 001.
[75] J. R. Ellis, G. B. Gelmini, J. L. Lopez, D. V. Nanopoulos, and S. Sarkar, Nucl. Phys. **B373**, 399 (1992).
[76] S. Dimopoulos, R. Esmailzadeh, L. J. Hall, and G. D. Starkman, Nucl. Phys. **B311**, 699 (1989).
[77] M. Pospelov, hep-ph/0605215.
[78] K. Kohri and F. Takayama, hep-ph/0605243.
[79] M. Kaplinghat and A. Rajaraman, Phys. Rev. D **74**, 103004 (2006).
[80] J. R. Ellis, D. V. Nanopoulos, and S. Sarkar, Nucl. Phys. **B259**, 175 (1985).
[81] E. Holtmann, M. Kawasaki, K. Kohri, and T. Moroi, Phys. Rev. D **60**, 023506 (1999).
[82] F. D. Steffen, J. Cosmol. Astropart. Phys. 09 (2006) 001.
[83] M. Kawasaki, K. Kohri, and T. Moroi, Phys. Rev. D **71**, 083502 (2005).
[84] T. Kanzaki, M. Kawasaki, K. Kohri, and T. Moroi, hep-ph/0609246.
[85] F. E. Paige, S. D. Protopopescu, H. Baer, and X. Tata, hep-ph/0312045.
[86] G. Corcella *et al.*, J. High Energy Phys. 01 (2001) 010; S. Moretti, K. Odagiri, P. Richardson, M. H. Seymour, and B. R. Webber, J. High Energy Phys. 04 (2002) 028; http://hepwww. rl.ac.uk/theory/seymour/herwig/.
[87] This program can be obtained from P. Richardson by email request.
[88] B. C. Allanach *et al.*, J. High Energy Phys. 03 (2001) 048; H. Baer, C. Kao, and X. Tata, Phys. Rev. D **51**, 2180 (1995); hep-ph/9410283; H. K. Dreiner, P. Richardson, and M. H. Seymour, J. High Energy Phys. 04 (2000) 008; hep-ph/9912407.
[89] H. Haber and G. Kane, Phys. Rep. **117**, 75 (1985).
[90] S. P. Martin, hep-ph/9709356.
[91] I. J. R. Aitchison, hep-ph/0505105.